Journal Pre-proof

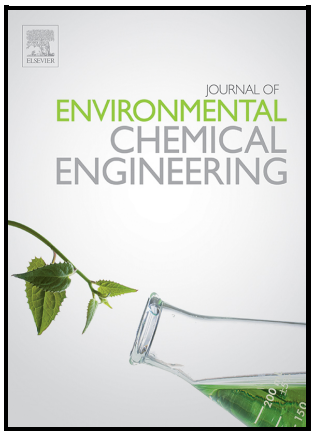

Mutual interaction of pyrolysis operating conditions and surface morphology for the electrochemical performance of biochar-modified screen-printed electrodes

Rocco Cancelliere, Pietro Mele, Lorenzo Bartolucci, Stefano Cordiner, Williane da Silva Freitas, Claudia Mazzuca, Barbara Mecheri, Laura Micheli, Vincenzo Mulone, Elisa Paialunga, Leonardo Severini

PII: S2213-3437(25)00172-1

DOI: https://doi.org/10.1016/j.jece.2025.115477

Reference: JECE115477

To appear in: *Journal of Environmental Chemical Engineering*

Received date: 23 September 2024
Revised date: 8 January 2025
Accepted date: 15 January 2025

Please cite this article as: Rocco Cancelliere, Pietro Mele, Lorenzo Bartolucci, Stefano Cordiner, Williane da Silva Freitas, Claudia Mazzuca, Barbara Mecheri, Laura Micheli, Vincenzo Mulone, Elisa Paialunga and Leonardo Severini, Mutual interaction of pyrolysis operating conditions and surface morphology for the electrochemical performance of biochar-modified screen-printed electrodes, *Journal of Environmental Chemical Engineering,* (2025) doi:https://doi.org/10.1016/j.jece.2025.115477

This is a PDF file of an article that has undergone enhancements after acceptance, such as the addition of a cover page and metadata, and formatting for readability, but it is not yet the definitive version of record. This version will undergo additional copyediting, typesetting and review before it is published in its final form, but we are providing this version to give early visibility of the article. Please note that, during the production process, errors may be discovered which could affect the content, and all legal disclaimers that apply to the journal pertain.

© 2025 Published by Elsevier Ltd.

Journal Pre-proof

Mutual interaction of pyrolysis operating conditions and surface morphology for the electrochemical performance of biochar-modified screen-printed electrodes

Rocco Cancelliere [a,c,1,*], *Pietro Mele* [b,1,*], *Lorenzo Bartolucci* [b], *Stefano Cordiner* [b], *Williane da Silva Freitas* [a], *Claudia Mazzuca* [a], *Barbara Mecheri* [a], *Laura Micheli* [a], *Vincenzo Mulone* [b], *Elisa Paialunga* [a], *Leonardo Severini* [a]

[a] Department of Chemical Science and Technologies, University of Rome Tor Vergata, Via Della Ricerca Scientifica 1, 00133 Rome, Italy

[b] Department of Industrial Engineering, University of Rome Tor Vergata, via del Politecnico 1, 00133, Rome, Italy

[c] ENEA, Technologies and Devices for Electrochemical Storage (TERIN-DEC-ACEL), Rome 00123, Italy

[1] These authors contributed equally to this work as co-first authors.

* Corresponding: rocco.cancelliere@uniroma2.it / rocco.cancelliere@enea.it, pietro.mele@uniroma2.it

Journal Pre-proof

ABSTRACT

The transition towards a low-emission economy requires advanced carbon-based materials for multiple applications.

This study aimed to correlate the temperature of intermediate pyrolysis with surface morphology and the electrochemical performances of biochar from hazelnut shells (HZS) and spent coffee grounds (SCG), obtained as by-products in bio-oil production. For this process, the biochar from HZS and SCG were produced using a lab-scale screw-type reactor designed in-house and operated in a semi-continuous regime, under two pyrolysis temperatures (450°C and 550°C) and thermal post-treatment (TT) durations of 10 and 60 minutes, respectively.

Physical-chemical characterization through Scanning Electron Microscopy (SEM), attenuated total reflection Fourier transform infrared spectroscopy (ATR-FTIR), cyclic voltammetry (CV), and electrochemical impedance spectroscopy (EIS) revealed distinct structural and electrochemical differences, unrevealing the fundamental importance of the feedstock selection. SEM analysis highlighted a more homogenous and open structure of HZS than SCG-based biochars. Electrochemical testing of biochar-modified screen-printed electrodes (BC-SPEs) demonstrated enhanced electron-transfer efficiency and diffusivity for HZS produced at 550°C, with the HZS_550 variant yielding a 1.5-fold increase in the heterogeneous electron transfer rate constant (k^0) and a 2-fold increase in diffusion coefficient (D_0) compared to SCG-SPEs. Notably, HZS_550-SPEs showed enhanced sensitivity for both reversible and non-reversible redox probes, achieving a limit of detection (LOD) in the micromolar (μM) range, halving the LOD of unmodified SPEs. These findings underscore that biochar's electron-transfer efficiency and texture are key factors driving its sensing performance. Crucially, these properties are governed by the formation of graphite-like sheet structures (GSSs), along with crystallinity and aromaticity, which develop from the condensation of amorphous carbon sheets during primary pyrolysis and are largely unaffected by TT.

Keywords: Pyrolysis; Biomass; Biochar; Electron-transfer process; Screen-printed electrodes.

Highlights:

- Biochar derived from the pyrolysis oil production of hazelnut shells (HZS) and spent coffee grounds (SCG) was evaluated for electrochemical applications.
- HZS biochar, produced at a pyrolysis temperature of 550°C, exhibited superior electrochemical performance compared to SCG-derived biochar.
- HZS biochar demonstrated a more uniform and open microstructure.
- Graphite-like sheets with well-organized packing in HZS biochar enhanced electron transfer and accordingly sensor performance.
- Electrodes modified with HZS biochar achieved nanomolar-level detection sensitivity, significantly surpassing unmodified electrodes.

Graphical Abstract:

Journal Pre-proof

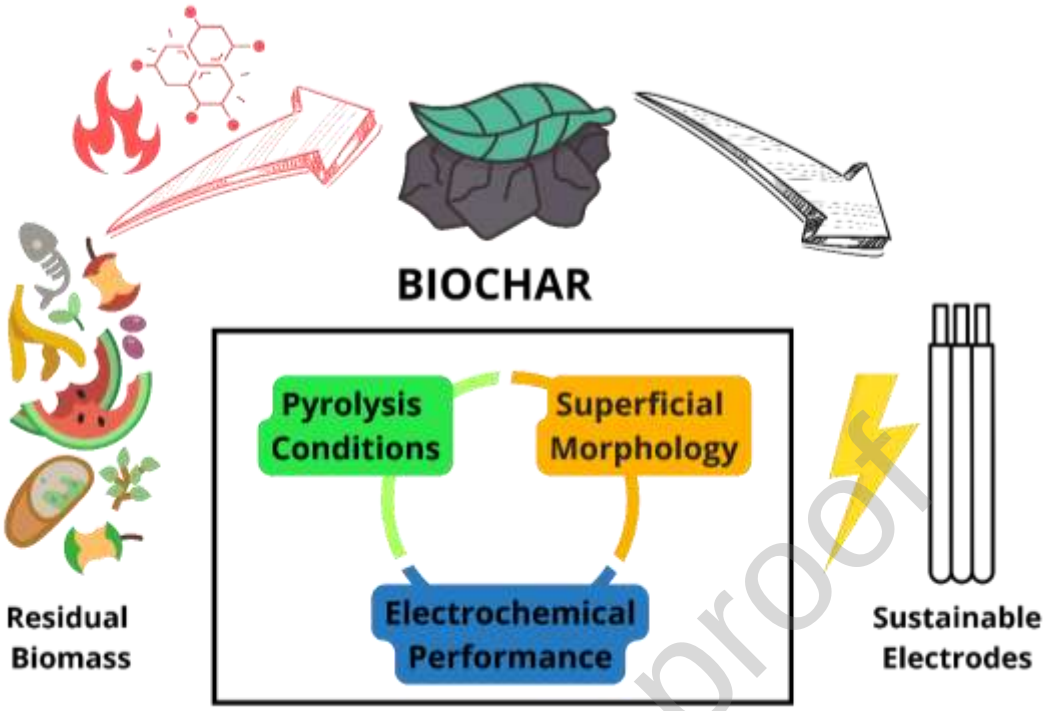

1. Introduction

Global warming and the correlated anthropogenic carbon dioxide (CO_2) emissions are urgent environmental problems, which can be described by one word “inexorable”. CO_2 emissions have increased by almost 3% yearly since 2000, leading Earth's ecosystems towards rapid and irreversible climate change. In the last decade, international institutions such as the IEA and the IPCC have suggested ambitious strategies to promptly mitigate anthropogenic emissions to reach near-zero or even net-negative emissions by 2050. In this overall scenario, biomasses and their thermal derivatives, especially biochar, represent an unprecedented opportunity. Biomass is a renewable, carbon-neutral, and highly abundant resource that exists in multiple forms, including agricultural by-products, biowaste, and organic residues [1][2]. Conversion of bio-residues to high-value materials, chemicals and biofuels, supports the circular economy and zero-waste production, reducing the pollution caused by their improper disposal [3].

In this context, thermochemical processes can efficiently convert low-value feedstocks into biochar, bio-oil and syngas. Pyrolysis is the thermal degradation of biopolymers under inert conditions and temperatures ranging from 300 to 600°C [4]. Operating conditions such as temperature, residence time and heating rate can be tuned to optimize the yields and the quality of the pyrolysis products [5], [6] [7]. Several reactor layouts,

Journal Pre-proof

such as auger reactors, fixed and fluidized beds and ablative reactors can be employed for the pyrolytic conversion of biomasses [8], [9]. The reactor configuration has a strong impact on the heat and mass transfer of the process, which in turn, influences the characteristics of pyrolysis products [10].

Biochar, the carbon-rich product of pyrolysis, offers promising applications across different fields (i.e., agriculture, environmental remediation, energy storage, conversion technologies and electrochemical sensing) due to its high surface area, porosity, and excellent electrical conductivity [11], [12], [13], [14], [15], [16], [17], [18], [19], [20] [21], [22], [23], [24]. In electrochemical sensing, biochar emerges as a sustainable alternative to carbon black (CB), whose production from hydrocarbon combustion incurs significant environmental costs, including greenhouse gas emissions and health risks [25], [26], [27]. As an electrode material, biochar enhances electrochemical reactions by facilitating rapid electron transport, which improves sensor sensitivity and response time [28], [29]. Its porous structure and extensive surface area provide efficient analyte adsorption, crucial for detecting trace levels in complex matrices like environmental and biological samples. Additionally, biochar's biocompatible surface is ideal for immobilizing bioreceptors (e.g., enzymes, antibodies), enabling the design of versatile electrochemical platforms with high specificity for a broad range of targets [30], [31]. These properties make biochar a valuable and eco-friendly choice for advancing (bio)sensor technology [32], [33], [34].

Our research group has effectively utilized biochar by incorporating it into the construction process of electrochemical (Bio)sensing devices that rely on screen-printed electrodes (SPEs). Produced by depositing conductive materials (i.e., graphite, graphene, metals etc.), onto non-conductive substrates (i.e., graphite, graphene, etc.) or metal inks (i.e., gold, silver, etc.), SPEs are low-cost, widely used sensors that enable mass production [31]. Their flexibility, disposability, and suitability for miniaturization make them ideal for point-of-care diagnostics and in-situ applications.

Pyrolysis conditions are known to be critical in defining the quality and potential applications of biochar [35], [36]. Numerous studies have examined the influence of pyrolysis temperature, duration, and heating rate on yield and surface morphology, consistently demonstrating that more intense pyrolysis conditions result in increased specific surface area and pore volume [37], [38]. Physical and chemical activation, along with thermal modification, further expand biochar's application scope [35], [39]. Mendonça et al. [40] reported

Journal Pre-proof

that thermal treatment effectively refines surface morphology, porosity, functionality, and reactivity, enhancing oxygen removal, surface area, and microporosity, which significantly improve adsorption and reactivity.

Although the literature on biochar is expanding, and **Table 1** reports a short list of the latest work in the field, a comprehensive understanding of its properties and challenges in electrochemical applications remains incomplete.

Table 1: Overview of the most impactful and recent applications of biochar in electrochemical sensing.

Feedstock	Pyrolysis Condition (°C)	Sensing Application	Ref.
BSG	600	Nitrite	[32]
PIW	1200	Neurotransmitters	https://doi.org/10.1016/j.chemosphere.2023.137884[41]
ES	1200	Phenol Moieties	[25]
NB	600	Malathion	[42]
SB	700	Copper (II)	[43]
SB	400	Paracetamol	[44]
CS	800	CAP	[45]
CC	800	Glucose	[46]
SF-1+AV	500	PM	https://doi.org/10.1016/j.chemosphere.2024.141151[47]
MO	400	CP	[48]
TR	300	Lead (II)	[49]
CaC	500	Glucose	[50]

Acronyms: brewers' spent grain (BSG), paper industry waste (PIW), eucalyptus scraps (ES), non-specified biomass (NB), sugarcane bagasse (SB), corn straw (CS), chloramphenicol (CAP), crop corn (CC), starfish (SF-1), aloevera (AV), polystyrene microplastics (PM), *Moringa oleifera* (MO), carbaryl pesticides (CP), tea residue (TR), castor cake (CaC).

The present work aims to investigate the cross-relationship between operating conditions, surface morphology, and electrochemical performances of biochars. Therefore, it tries to answer the question of how the electrical properties of biochar relate to the morphology, the primary feedstock, the process conditions, the reactor layout, and the scale-up.

For this purpose, two residual biomasses, hazelnut shell (HZS) and spent coffee grounds (SCG), were processed and converted to biochar. The first represents one of the most diffused agro-industrial wastes in the Mediterranean and Middle-East countries. At the same time, the second is the brewing residue of coffee powder, the most traded good in the world after crude, whose consumption is expected to increase by 2.2% to 177.0 million 60 kg bags for the year 2023/2024 [51] [52]. Firstly, HZS and SCG have been pyrolyzed employing a laboratory-scale screw-type reactor at the pyrolysis temperatures of 450°C and 550°C and a

residence time of 15 seconds. The operating conditions used are typical of intermediate pyrolysis. The biochar pyrolyzed at 550°C was thermally post-treated, operating the reactor in batch mode, considering holding times of 10 and 60 minutes. Scanning Electron Microscopy (SEM), and Fourier Transform Infrared (ATR-FTIR) techniques were employed for morphological characterization of the pyrolysis char and thermal upgrade. Then, these materials were used as SPE modifiers and electrochemically characterized utilizing EIS, CV, and amperometry. The analytical capabilities of BCs-modified-SPEs were evaluated to analyze both reversible and non-reversible electroactive probes with significant environmental implications. This work contributes towards understanding the use of biochar for electrochemical applications to support the development of a carbon bio-economy and the implementation of multi-product biorefineries.

2.0 Materials and Methods

The following methodology was implemented to understand the mutual interaction between the superficial properties of biochar and the operational conditions of pyrolysis. Firstly, dried feedstock has been characterized through thermogravimetric and elemental analysis (2.1). After that, a screw-type reactor was operated for both intermediate pyrolysis in semi-continuous and thermal upgrading of the biochar in semi-batch operations, as described in section 2.2. Subsequently, biochar samples (HZS and SCG) were characterized to understand the effect of the primary pyrolysis treatment and thermal post-treatment on the elemental composition and surface morphology (Section 2.3). Commercial biochar (BC, 100% pure virgin wood certified PEFC, Nera Biochar Srl, Turin, Italy) was used as a standard for the validation of HZS and SCG electrochemical performances. Consequently, the electrochemical performance of biochar-SPES was outlined through CV, square wave voltammetry (SWV) and EIS. The theoretical background and experimental details of the analysis of the electrochemical performances of SPEs are reported in section 2.4.

2.1 Materials

All the chemicals from commercial sources were of analytical grade. Ethanol, potassium ferri/ferrocyanide, p-benzoquinone, and hydroquinone were purchased from Merck (Merck KGgA, Steinheim, Germany). The buffer solution used was 0.05 M phosphate-buffered saline (PBS), 0.1 M KCl, pH = 7.4.

Journal Pre-proof

HZS were supplied from Assofrutti S.r.l. (Viterbo, Italy) a consortium of nut producers in the Lazio region. HZS were milled using a knife mill (Retsch GM-100) before being processed. No further drying was required since HZS was received with a 9.9 wt. % residual moisture content.

Spent coffee grounds (SCG), a blend of arabica/ robusta 40:60 by weight, as specified by the producers, were collected from the coffee shop of the Department of Industrial Engineering of the University of Rome 'Tor Vergata'. SCG was dried in a static oven for 12 h. Before being subjected to intermediate pyrolysis, both the feedstocks were sieved to obtain a particle size between 500 µm and 850 µm.

Thermogravimetric and elemental analyses of the feedstocks are reported in **Table 1**, displayed in the first section of the results and discussion section.

2.2 Pyrolysis Set-up

The intermediate pyrolysis of HZS and SCG was conducted using a 300 g/h screw-type reactor in a semi-continuous operation mode. This reactor configuration was specifically chosen to prevent any char contamination. A sketch of the experimental setup is reported in Figure 1. The temperature range explored in this study was 450-550°C, with the vapors/gas temperature at the reactor outlet i.e. inlet of the vapor/gas filter, chosen as representative of the process. Nitrogen gas was introduced at a rate of 1.5 NL/min to maintain an inert atmosphere. The solid biomass was conveyed in the reaction zone through the shaftless screw. The solid particle residence time was estimated in the order of 30 seconds. The calculated heating rate was 80-100°C/s, and the holding time at the pyrolysis temperature was 15 seconds. Bio-oil was collected through a three-stage condensing system and cooled to 0°C using water-ethanol (50:50 vol/vol) solutions. Char and bio-oil yields were determined gravimetrically, while the pyrolysis gas yield was calculated by difference. The biochar samples obtained at 550°C have been processed to remove residual moisture and volatile matter further. For the thermal post-treatment of biochar, the reactor was operated in a semi-batch mode. In a typical run, 2 g of HZS/SCG samples were loaded in a ceramic tray placed on the top of the sand bed of the hot-sand filter of the reactor. The filter was heated at 100 °C/min up to 550°C, maintaining the inert atmosphere throughout the test. The temperature was kept constant for 10 and 60 minutes, and the system was cooled down. Volatile/moisture further removal was measured by the weight difference of the samples before and after the post-treatment. The operating conditions set for this study were proven to be very efficient for the thermochemical conversion of

Journal Pre-proof

residual biomass in our previous investigations [53]. Additional details about the pyrolysis rig can be found in [5].

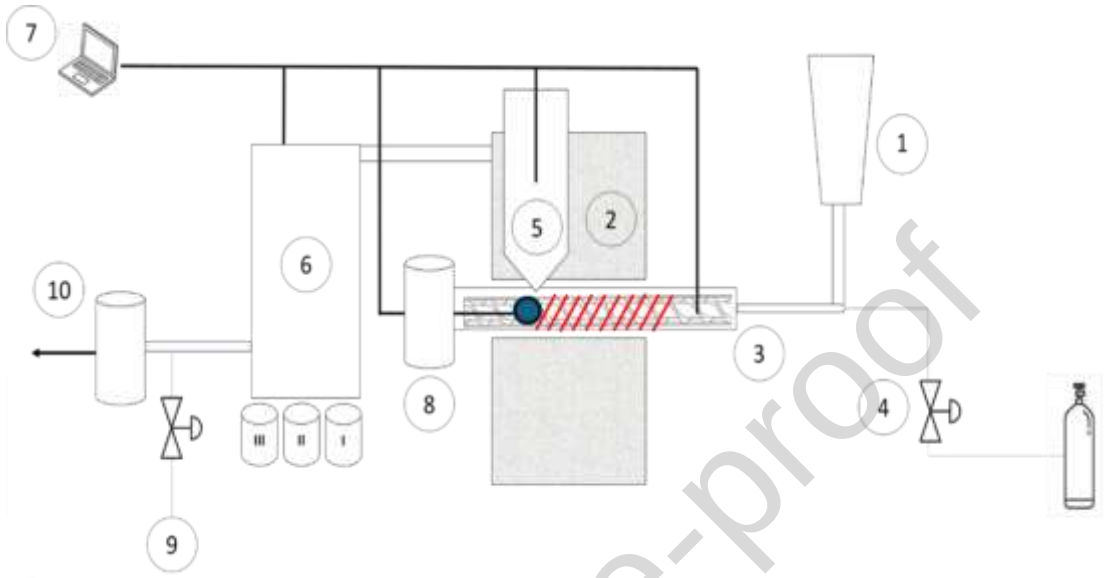

Figure 1 Scheme of the screw-type reactor employed for intermediate pyrolysis tests. The following elements are present: 1) Feed hopper; 2) Electrical-heated ovens; 3) Shaftless screwdrivers; 4) Mass flow controllers; 5) Hot-sand filters; 6) Bio-oil condensers; 7) Data acquisition system; 8) Biochar tanks; 9) Pyrolysis-gas samplings; 10) Vent. In blue is indicated the location where was placed the thermocouple representative of the pyrolysis temperature.

The samples obtained, and their labelling, are listed in **Table 2**.

Table 2 Labels of the samples, the object of this study.

Biomass Source	Pyrolysis Temperature	Post-treatment	Sample's Label
Hazelnut shell	450°C	none	HZS_450
Hazelnut shell	550°C	none	HZS_550
Hazelnut shell	550°C	550°C, 10 min	HZS_550_TT10
Hazelnut shell	550°C	550°C, 60 min	HZS_550_TT60
Spent coffee grounds	450°C	None	SCG_450

Journal Pre-proof

Spent coffee grounds	550°C	None	SCG_550
Spent coffee grounds	550°C	550°C, 10 min	SCG_550_TT10
Spent coffee grounds	550°C	550°C, 60 min	SCG_550_TT60

2.3 Ultimate and Proximate Analysis

Proximate analysis was conducted following ASTM E914, utilizing the TGA 701 manufactured by LECO Corp. The analyses were carried out following UNI EN ISO 18122:2016, ISO 18122:2015, and ISO 18123:2015 guidelines. The thermal program employed consisted of a heating ramp at 10 °C/min from ambient temperature to 105 °C for moisture determination, maintained until a constant mass was achieved. Subsequently, a 15 °C/min ramp under a nitrogen atmosphere up to 550 °C was applied for volatile matter determination, followed by a final 15 °C/min ramp under a nitrogen and oxygen atmosphere for ash evaluation. The fixed carbon content was determined by difference. The CHN(O) analysis was carried out using Elemental Macro's Vario MACRO-cube analyzer. Calibration of the instrument with the sulfanilamide standard and the analysis adhered to the ISO 16948:2015. The oxygen content of the samples was calculated by difference, taking into account the ash content previously measured by proximate analysis.

2.4 Scanning Electron Microscopy (SEM) and X-ray diffraction (XRD) analysis

The morphology of the biomass sources and thermally treated biochar was analyzed using Leo SUPRA™ 35 field emission scanning electron microscope (FE-SEM), Carl Zeiss, Oberkochen, Germany. Before the measurements, the raw biomass was sputtered with Au using a coater K550X (EMITECH) with a 25 mA current for 1 min and 30 s to obtain a coating layer ~ 15 nm thick. At the same time, the thermally treated samples were analyzed in their bare conditions, without an Au coating layer. X-ray diffraction (XRD) patterns were recorded using a Philips PW1730 diffractometer with Cu Kα radiation (λ =1.5406 Å).

2.5 ATR-FTIR spectroscopy analysis

FTIR absorption spectra of biochar samples were acquired with the Thermo-Scientific instrument (model Is50) (Thermo Scientific Inc., Madison WI USA) in Attenuated Total Reflectance (ATR) mode using a single

Journal Pre-proof

reflection diamond cell. Spectra were recorded from 4000 to 500 cm^{-1}, averaging over 32 scans with a resolution of 2 cm^{-1}. All experiments were performed in triplicate, yielding consistent and reproducible results. Spectra are baselined where no absorbance peaks are present (at about 1950 cm^{-1}).

2.6 Electrochemical Apparatus

Using a PalmSens4 Instrument (PalmSens, Netherlands), analyses by CV, chronoamperometry (sigla), SWV, and EIS) were conducted. A Hielscher UP200 St-Ultrasonic Transducer was employed in the biochar dispersion preparation process.

2.7 Preparation of Biochar-modified SPEs

Initially, SPEs were amperometrically pre-treated by applying a steady anodic potential of +1.7 V for 180 s in a 0.05 M phosphate buffer + 0.1 M KCl, pH 7.4 solution. Following a rinsing process (100µL, three times) to eliminate any potential salt residues, 6µL of a Biochar dispersion (1 mg/mL in 1:3 v/v ethanol-water solution) was drop-cast onto the working electrode (WE) surface of SPEs. The dispersion had been previously prepared using an ultrasonic transducer (200 W, 26 kHz, 30 minutes). The deposited solution is dried under controlled conditions (15 minutes at 38 °C). Additionally, the impact of depositing multiple layers of biochar onto SPEs was investigated; in this case, the procedure above reported was repeated as many times as the desired number of coatings.

2.8 Theoretical methods

The electrochemical layer-by-layer characterization (LbL-EC) of biochar-modified SPEs (Bio-SPEs) was conducted following the reversible redox process of ferro-ferricyanide: $[Fe(CN)_6]^{3-} + 1e^- \rightleftarrows [Fe(CN)_6]^{4-}$. Electrochemical parameters, such as the heterogeneous electron transfer constant (k^0), diffusion coefficient (D_0), peak-to-peak separation (ΔE) and current peak ratio (Ipa/Ipc) were calculated. More precisely, k^0 was evaluated voltammetrically according to Marcus' theory (Eq.1) and impedimetrically ($k^{0'}$) following Randles's theory (Eq.3) [32]. Whereas D_0 was evaluated using the Randles-Sevcik equation (Eq.4):

Journal Pre-proof

$$k^0 = \varphi\sqrt{\frac{D_0 \pi v n F}{RT}\left(\frac{D_R}{D_O}\right)^{\alpha}} \quad \text{(Eq.1)}, \quad \varphi = \frac{(-0.6288+0.0021\cdot\Delta E)}{(1-0.0170\cdot\Delta E)} \quad \text{(Eq.2)}, \quad k^{0\prime} = \frac{(RT)}{(n^2F^2ACR_{ct})} \quad \text{(Eq.3)}$$

where D_O and D_R are the diffusion coefficients ($cm^2\ s^{-1}$) for ferricyanide (D_O) and ferrocyanide (D_R), v is the scan rate ($mV\ s^{-1}$), n is the number of electrons involved in the process, T is the temperature (K), F is the Faraday constant ($C\ mol^{-1}$), R is the universal gas constant ($J\ K^{-1}mol^{-1}$) and α the dimensional transfer coefficient. The parameter φ is based on the potential difference between anodic and cathodic peaks (ΔE).

$$I_p = (0.4463)nFAC\sqrt{\frac{nFvD_0}{RT}} \quad \text{(Eq.4)}$$

where I_p is the current peak, n is the number of electrons exchanged, F is the Faraday constant (mol^{-1}), R is the universal gas constant ($J\ K^{-1}mol^{-1}$), A the electrode area (cm^2), C is the analyte concentration ($mol\ cm^{-3}$), D_0 the diffusion coefficient ($cm^2\ s^{-1}$), and v the scan rate ($mV\ s^{-1}$).

3. Results and discussion

In accordance with the methodology outlined earlier, this section presents the findings of the investigation. Section 3.1 details the feedstock characterization, the product yields of pyrolysis experiments (450°C, 550°C) and BC thermal treatment at 550°C. Afterwards, thermogravimetric and elemental analysis, scanning electron microscopy and FTIR-ATR spectroscopy analysis are shown, underlining the beneficial effect of the post-treatment on the superficial morphology of the BC, in Sec. 3.2. Finally, the optimization of BC dispersion conditions for the manufacture of SPEs (3.3.1), the electron-transfer capabilities of SPEs (3.3.2) and the performance of BCs-modified SPE as sensing platforms (3.3.3) are discussed.

3.1 Feedstock Characterization

The results of thermogravimetric and elemental analysis of the HZS and SCG obtained via intermediate pyrolysis are presented in Table 3. The results of characterization reveal that the thermochemical conversion of the feedstock object of this study is promising since the moisture content is lower than the 10 wt. %, the upper limit that is generally recommended for pyrolytic conversion of biomass [54][55][56]. A slight difference between HZS and SCG is the ash content, as shown by TGA, and the nitrogen content, as confirmed by the elemental analysis. The reported data are in line with the ones already present in the literature.

Journal Pre-proof

Table 3. Thermogravimetric and elemental analysis of the HZS and SCG feedstocks after drying.

Thermogravimetric Analysis		
	HZS	**SCG**
Moisture (wt. %)	9.99 ± 0.51	4.67 ± 0.05
Volatile Matter (wt. %)	67.23 ± 0.23	76.70 ± 0.07
Fixed Carbon (wt. %)	22.11 ± 0.54	21.09 ± 0.08
Ash (wt. %)	0.67 ± 0.09	2.19 ± 0.02
Elemental analysis		
	HZS	**SCG**
C (wt. %)	47.57 ± 0.11	51.34 ± 1.13
H (wt. %)	6.37 ± 0.66	6.91 ± 0.65
N (wt. %)	0.06 ± 0.01	2.13 ± 0.25
S (wt. %)	0.01 ± 0.01	0.08 ± 0.02
O (wt. %) a	47.31 ± 0.84	37.35 ± 2.05

a. Calculated by difference.

Product yields of intermediate pyrolysis of HZS and SCG are reported in Figure 2. As expected, pyrolysis temperature has a notable impact on product yields. The increase in pyrolysis temperature enhances the reaction rates of both heterogeneous and homogeneous reactions. However, biochar yield undergoes a slighter reduction with the temperature, remaining in the range of 18.9-21.0 wt.% and 17.7-23.1 wt. % for HZS and SCG, respectively. The temperature rise has a significant impact on bio-oil and non-condensable gas. This behaviour could be due to secondary volatile cracking reactions, which become predominant at elevated temperatures [57], [58]. Similar results for SCG and HZS pyrolysis can be found in the literature. Ali et al. [59] reported a biochar yield of 30.0-35.2 wt. % and oil yield of 35.2 – 40.0 wt. % for HZS pyrolysis in the temperature range of 400-600°C. Kelkar et al. [54] reported biochar yields of 15-22 wt. % for SCG fast pyrolysis carried out with a screw-conveyor reactor in a temperature range of 450-550°C.

Journal Pre-proof

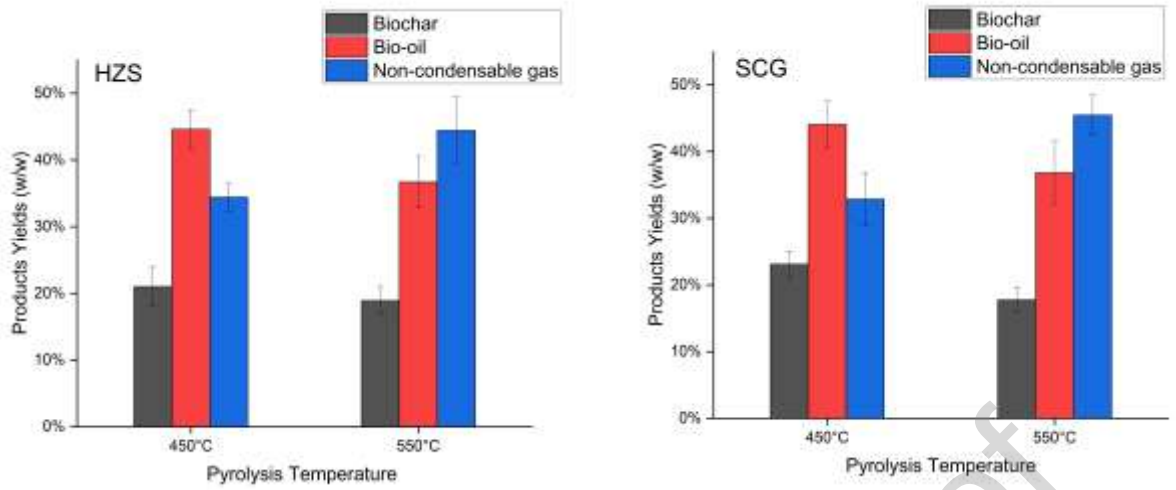

Figure 2. Products yields of the intermediate pyrolysis of HZS (left) and SCG (right).

Table 4 shows the weight loss during the thermal post-treatment of biochar. As expected, the increase in treatment time led to a higher weight loss in the process. Notably, the weight loss for HZS is lower if compared to SCG. This can be partly attributed to the lower amount of residual volatiles of HZS biochar concerning SCG. Another significant difference between HZS and SCG is the incremental weight loss with increased thermal treatment time. While for HZS the weight loss at 60 minutes of thermal treatment is more than double if compared to the weight loss at 10 minutes, for SCG the weight losses at the two different residence times are similar. This suggests that two different feedstocks have different thermal kinetics. Hence, the residence time and pyrolysis temperature need to be set carefully to maximize the electrochemical properties of biochar.

Table 4. Weight losses of the thermal post-treatment of biochars, carried out in semi-batch mode.

Feedstock	Weight Loss (wt. %)
HZS_550_TT10	5.8 ± 0.3
HZS_550_TT60	12.2 ± 0.1
SCG_550_TT10	29.7 ± 5.3
SCG_550_TT60	31.9 ± 4.1

Journal Pre-proof

3.2 Biochar elemental and proximate analysis

Table 5 and **Figure 3** show the thermogravimetric and elemental analysis results for the pyrolysis char obtained at 450°C and 550°C. As evident, an increase in pyrolysis temperature leads to the increase of fixed carbon fraction (on a dry basis). The enrichment of carbon is attributed to dehydration, decarbonylation and decarboxylation reactions that are more intense at higher temperatures [60]. The fixed carbon content of HZS biochars is remarkable, consistent with previous investigations on various nutshells and fruit stones' pyrolysis residues [61]. Nitrogen and ash content of biochar are significantly different between the two feedstocks; this is clearly due to the composition of the raw biowaste. Notably, nitrogen is considered particularly attractive in catalysts for electrochemical applications [62].

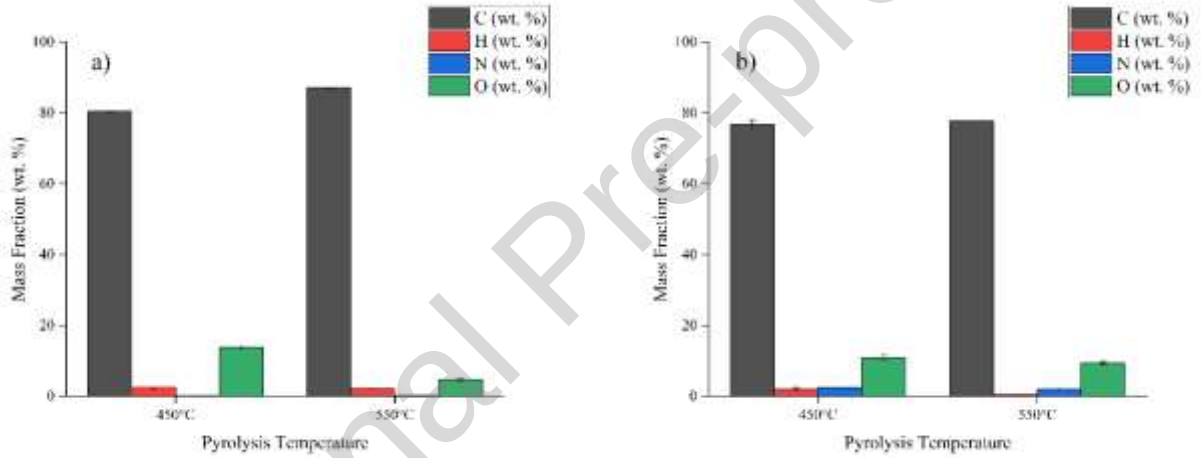

Figure 3 Elemental analysis of the HZS (a) and SCG (b) biochars obtained from intermediate pyrolysis at 450°C and 550°C.

The results of the characterization of the post-treated HZS_550 and SCG_550 biochars are reported in **Table 5**. As expected, the volatile matter content decreases steadily with the increase of thermal treatment time, while fixed carbon and ash content increases. Therefore, from proximate analysis is possible to conclude that thermal treatment at 550°C was effective for the partial removal of volatile matter and moisture. As a result of moisture reduction, oxygen and hydrogen content decreases. Similar results in terms of the elemental composition of thermally treated biochar were found in the literature. Zhu et al. [63] performed the thermal treatment at 700°C of softwood sawdust biochar, obtaining post-treated biochar with a carbon content of up to 91.2 wt. % and residual oxygen content of 3.81 wt. %. Mendonça et al. [40] investigated the thermal treatment of sugarcane sawdust/straw mix biochar under various temperatures (400, 600, 800°C) and a holding time of 1 hour, under

Journal Pre-proof

a nitrogen atmosphere. They obtained a similar trend of carbon enrichment and oxygen removal with the temperature.

Table 5. Thermogravimetric and elemental analysis of the biochars, before and after TT. The standard deviation values, calculated from the five most representative measurements for each sample, are reported.

Sample	Moisture (wt. %)	Volatile Matter d.b (wt. %)	Fixed Carbon d.b. (wt. %)	Ash d.b. (wt.%)	C (wt. %)	H (wt. %)	N (wt. %)	O (wt. %)
SCG_550	7.6± 0.6	23 ± 1	66 ±3	10 ±1	78 ± 2	0.63 ± 0.05	2.0 ± 0.2	9.3 ± 0.4
SCG_550_TT10	3.1±0.4	8±1	81 ± 4	10.5± 0.4	81 ± 2	0.6 ±0.1	2.4±0.2	5.4 ± 0.4
SCG_550_TT60	3.0 ± 0.1	5±2	82 ± 2	11.0 ± 0.1	82 ±1	0.5±0.1	2.5± 0.2	3.6 ± 0.1
HZS_550	7.9 ± 0.4	16±1	78 ± 1	5.7±0.3	87 ± 1	2.1 ±0.01	0.23± 0.03	4.8 ±0.1
HZS_550_TT10	5.0 ±0.7	10±1	88 ± 1	6.1± 0.2	8 ± 2	1.6 ± 0.10	0.25± 0.02	4.1± 0.3
HZS_550_TT60	4 ± 0.1	6.7±0.4	88.1 ± 0.5	6.4± 0.1	88± 1	1.4±0.1	0.26 ±0.01	3.8 ± 0.2

The morphology of the biomass source (feedstock) and biochar was investigated by SEM analysis. SEM micrographs for SCG and HZS evidenced different morphologies (Figure S3a-c). SCG is characterized by large aggregates (~ 60 µm) of particles with similar shape and size ranging between 5 and 10 µm. HZS showed an irregular morphology with fragmented particles of heterogeneous dimensions (5 – 50 µm) (Figure S3d-f). Furthermore, a few cavities can be found at the surface of the larger particles (Figure S1f). The observed features are aligned with other SEM analyses reported for similar feedstocks without chemical and thermal activation processes [64] [65] [66]. After pyrolysis at 450 °C, particle size decreased for both SCG_450 and HZS_450 (Figure S4) due to the removal of the volatiles and carbonization of the biomass structure, promoting its fragmentation. At a higher pyrolysis temperature (550 °C), the presence of large pores becomes more evident for both SCG_550 and HZS_550 (Figure 4). Furthermore, HZS_550 exhibited a more homogeneous and open structure than SCG_550, which can be attributed to the lower volatile matter content and higher fixed carbon content, as reported in **Table 5**, in good agreement with previous reports [67].

Journal Pre-proof

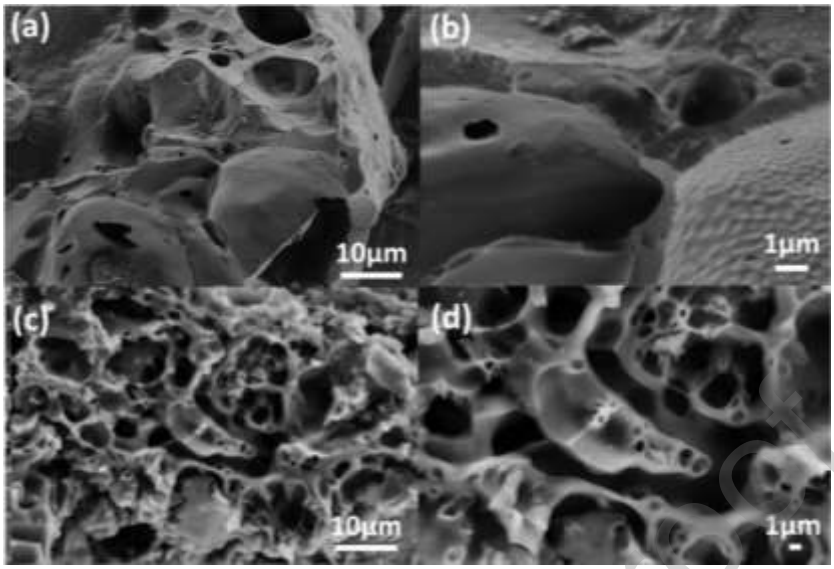

Figure 4 SEM micrographs of SCG_550 at a magnification of (a) 5 and (b) 25 kX and HZS_550 at (c) 5 and (d) 10 kX.

The thermal post-treatment influenced the morphology of both HZS_550 and SCG_550 biochar samples. For the SCG_550 sample, a 10-minute post-treatment caused the structure to transition into a multi-sized arrangement, with smaller particles distributed onto a porous framework. This trend persisted in the sample treated for 60 minutes, although partial fragmentation of the structure was observed..

In the case of HZS-based biochar (**Figure 6**), the 10-minute post-treatment resulted in smaller pores that were uniformly distributed across the primary structure (Figure 6 a-c). After 60 minutes of post-treatment, larger pores were observed (Figure 6 d-f) compared to HZS_550_TT10. These findings suggest that the extended post-treatment effectively facilitated volatile extraction and enhanced pore development in the biochar while maintaining a uniform porous architecture [68], [69].

The morphological differences observed for SCG- and HZS-based samples can be attributed to a less pronounced decrease in volatile content for HZS-based samples compared to SCG-based samples after the post-treatment. After a 10-minute post-treatment, 40.7% of volatiles were removed for HZS_550_TT10, compared to 66% for SCG_550_TT10. Following a 60-minute post-treatment, the removal increased to 54% for HZS_550_TT60 and 78% for SCG_550_TT60

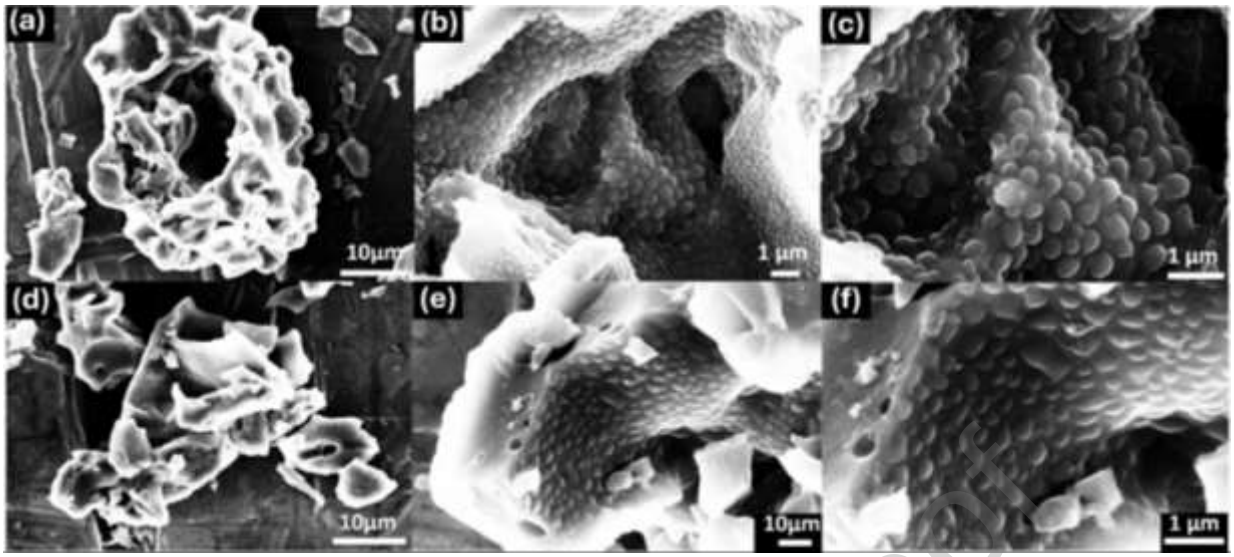

Figure 5. SEM micrographs for SCG_550_TT10 at a magnification of (a) 5, (b) 25, and (c) 50 kX, and for SGC_550_TT60 at (d) 5, (e) 25 and (f) 50 kX.

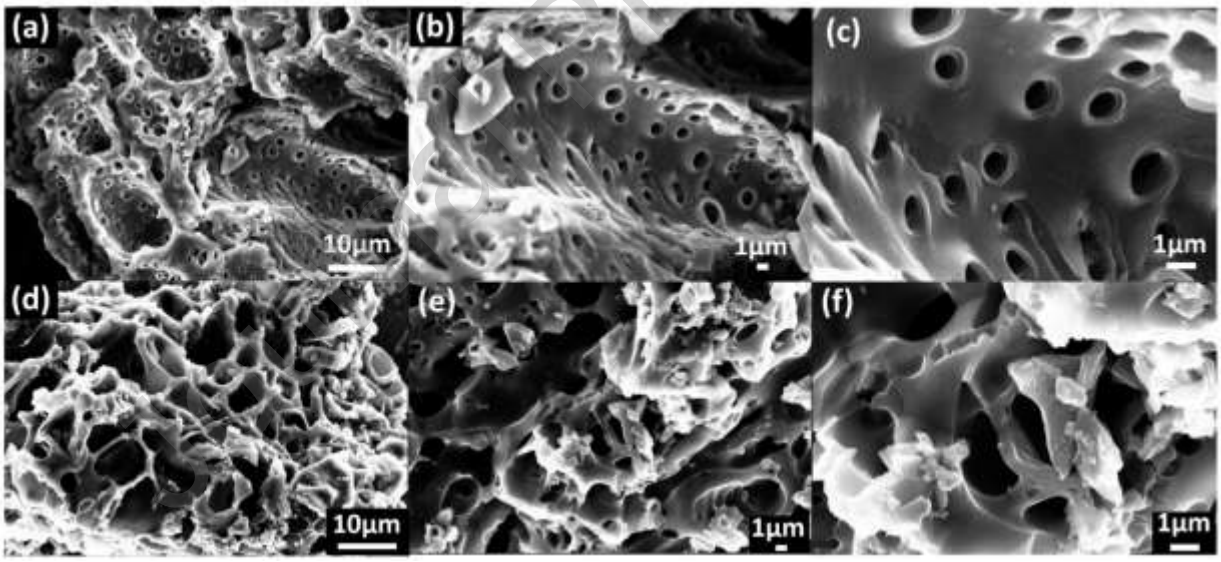

Figure 6. SEM micrographs at magnifications of 5, 10 and 25 kX of HZS_550_TT10 (in a, b and c) and HZS_550_TT60 (in d, e and f), respectively.

BET measurements are a widely accepted method to directly quantify porosity and surface area. However, it is noteworthy that accurate BET analyses are not usually reported in the studies dealing with chars obtained by fast pyrolysis, possibly due to the limitation of a fast-heating rate in removing volatiles and other impurities [70]. The issues found in recording N_2-adsorption-desorption for char obtained by fast pyrolysis have been

previously reported, demonstrating that the BET measurements can be compromised due to the presence of volatiles, ashes, and minerals causing pore clogging and requiring acidic leaching for impurities removal or activation [71]. Considering the purpose of valorizing biomass waste by adopting a direct and energy-saving approach, we have not performed further biochar purification or activation treatment. For all these reasons, the BET surface area analysis of the biochars has not been included in the manuscript.

After that, an ATR-FTIR analysis was carried out. As shown in **Figure 7,** all FTIR spectra of HZS and SCG biochar samples, after intermediate pyrolysis at 450°C and 550°C, show broad bands, characteristic of biochar [72]. A band near 3300 cm^{-1} is attributable to the stretching vibration of hydrogen-bonded hydroxyl groups [73]. The band at 1740 cm^{-1} was identified, for SCG samples only, with C=O stretching of carbonyl compounds (Figure 8, right panel). C=C stretching, in aromatic ring structures, and O-H bending, in functional groups and moisture, vibrations are responsible for bands at about 1430-1460 cm^{-1} and 1640 cm^{-1}, respectively. [73]. The band at 1030 cm^{-1} was attributed to the symmetric C–O stretching [74]. Two sharp peaks at 1240 cm^{-1} and 1160 cm^{-1} have been assigned to C–H stretching and OH deformation of COOH (if present as in SCG) or C–O stretching of aryl esters and asymmetric C–O stretching characteristic of C–O–C groups. The O–H bending of phenols was identified by the band 1375 cm^{-1}. The band at 875 cm^{-1} was attributed to the C–H bending aromatic CH out-of-plane deformation [73]. The bands near 1430 cm^{-1}, 1365 cm^{-1} and 870 cm^{-1} arise definitively from calcite in case of HZS [75]. Moreover, for SCG samples only, the asymmetric (2920 cm^{-1}) and symmetric (2850 cm^{-1}) C–H stretching bands were visible and associated with aliphatic functional groups (Figure 7, right panel). These results show no significant differences between samples treated at 450°C and 550 °C, but as shown in Figure S5, the molecular structure of the starting HZS and SCG biomass is drastically altered after intermediate pyrolysis.

Journal Pre-proof

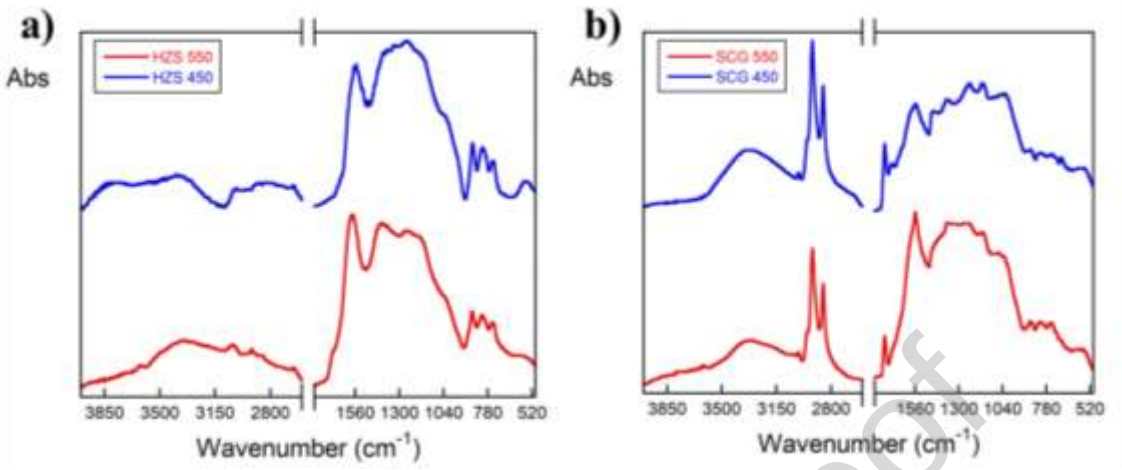

Figure 7. ATR-FTIR spectra of HZS (a) and SCG (b) biochar samples after intermediate pyrolysis at 450°C (blue) and 550°C (red).

FTIR characterization of the post-treated HZS and SCG biochar samples, for 10 or 60 minutes, is reported in **Figure 8** . In the case of HZS, the spectrum, highlighted in the region between 1800 and 525 cm^{-1}, shows the same fingerprint profile already described for the samples dealt with intermediate pyrolysis, not finding any substantial differences in the molecular structure of the samples after this treatment. In the case of the SCG sample, the bands associated with aliphatic functional groups and C=O stretching of carbonyl compounds

Journal Pre-proof

disappeared, after this last step (Figure 9, right panel). This might indicate that after the procedure, the removal of components adsorbed on the surface such as aliphatic hydrocarbons and oily substances has occurred.

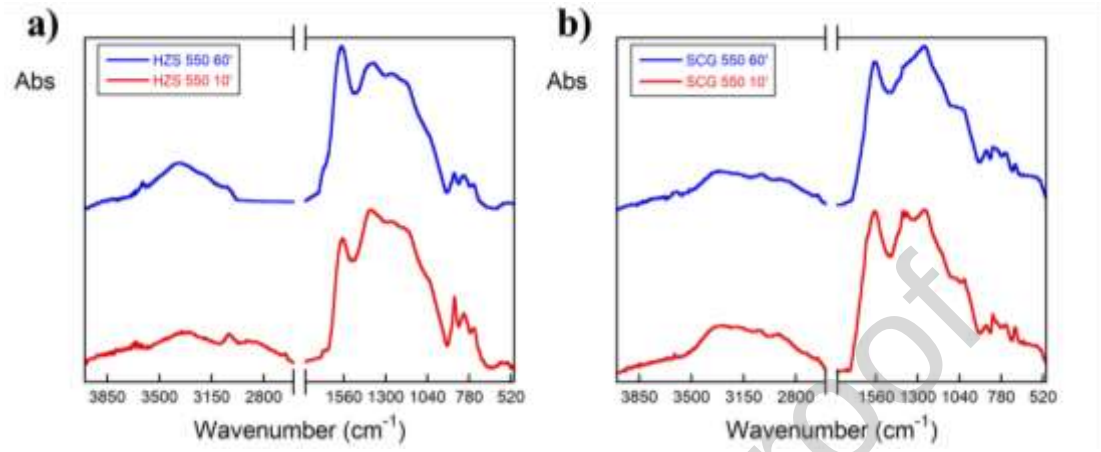

Figure 8. ATR-FTIR spectra of HZS (left panel) and SCG (right panel) biochar samples after thermal post-treatment at 550°C for 10 (red) and 60 (blue) minutes.

Furthermore, as shown in Figure S5, bands between 2800 and 3000 cm^{-1} represent C–H stretching vibrations. For the HZS biomass spectrum, these bands are attributable to aliphatic moieties present in the wooden composition of the hazelnut shells. Just after the intermediate pyrolysis treatment, these bands decrease drastically, as shown in Figure 7, almost disappearing, to demonstrate an almost total pyrolysis of the sample. For SCG biomass spectrum (Figure S5), these bands are attributable to aliphatic moieties of polysaccharides in spent coffee grounds, such as galactose, arabinose, glucose, mannose and other polysaccharides in various proportions and adsorbed aliphatic hydrocarbons and oily substances [76]. It should be highlighted that these bands remain almost unchanged after the intermediate pyrolysis treatment, as visible in Figure 7, due to incomplete pyrolysis, but disappear after the post-treatment for 10 and 60 minutes (see Figure 8).

3.3 Biochar electrochemical characterization

To determine the electrochemical properties of the BCs used for this study, a meticulous examination of their dispersion properties was conducted. Diverse solvents, including water (H_2O), ethanol (EtOH), propanol (PrOH), dimethyl sulfoxide (DMSO), and water mixtures (1:1 v/v) thereof, were evaluated in this regard. The outcomes obtained characterizing electrochemically (CV and EIS) SPEs modified with each HZS dispersion

Journal Pre-proof

are illustrated in **Figure 9**. However, comparable results were obtained for SCG. Visual examination revealed that, of all the dispersion samples examined, the one produced in H_2O: EtOH exhibited the greatest promise in terms of current (Ip) and charge transfer resistance (Rct) recorded; consequently, a more comprehensive investigation was undertaken to examine various volumetric ratios (1:1. 1:2, 1:3, 1:4 v/v) [77].

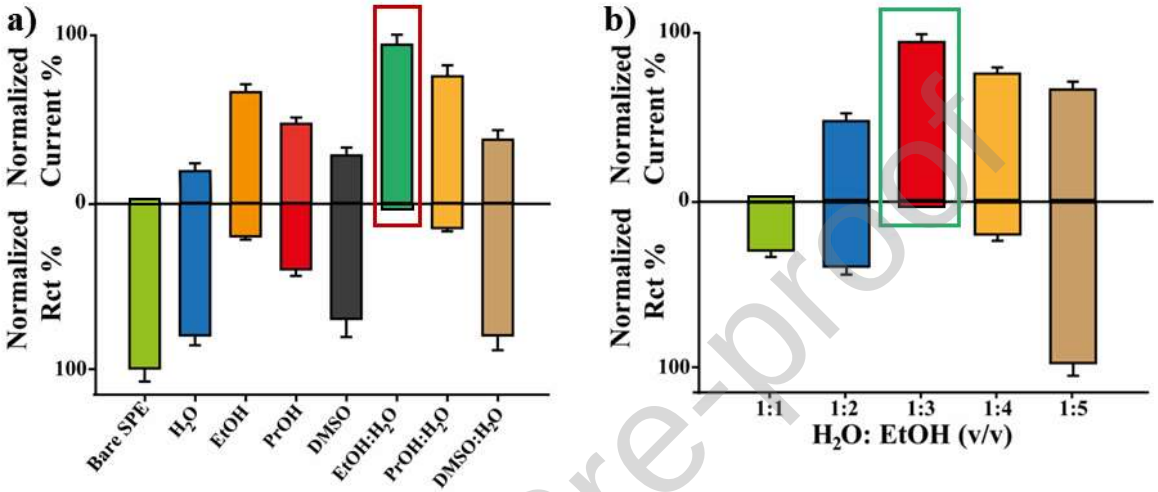

Figure 9. Electrochemical optimization of HZS_550 dispersion conditions. In a) CV and EIS outcomes derived from the analysis of HZS_550-modified SPEs in which BC was dispersed in H_2O, EtOH, PrOH, DMSO and the dilution in H_2O of the last three at 1:1 ratio, respectively. After determining that EtOH:H_2O produced the most effective dispersing solvents, various volumetric ratios, namely 1:1, 1:2, 1:3, 1:4 and 1:5 v/v, were examined; the corresponding outcomes are detailed in b). At least six electrodes (n=6) were analyzed for each experimental condition (RSD%<12).

Upon careful examination of **Figure 9**, it becomes evident that the dispersion in H_2O: EtOH (3:1 v/v) provides the most favorable balance between the electrochemical output recorded (current/impedance), repeatability and solution sustainability; thus, it was selected as the dispersing condition.

Once the dispersion condition of BCs, an in-depth electrochemical study to investigate the effectiveness of these carbonaceous materials as SPE conductive enhancers was carried out. To that end, the electrochemical performances of bare electrodes were compared with those of commercial BC, HZS_450, HZS_550, SCG_450, and SCG_550-modified SPEs. Initially, the background current was measured amperometrically (0.4 V, 180 s) by examining six different electrodes (n = 6) in a 50 mM KCl solution for each platform. The following current results were obtained: 140 ± 18, 57 ± 10, 9 ± 1, 55 ± 5, 45±4, 41±5 nA for bare and BC,

Journal Pre-proof

HZS_450, HZS_550, SCG_450, and SCG_550-modified electrodes, respectively. In addition, it was possible to determine that the addition of BCs allowed for the production of a more reliable electrochemical device with a significant reduction in capacitive current by estimating the signal-to-noise ratio and reproducibility using the standard deviation. Electrochemical measurements, conducted with or without the addition of 10 mM $[Fe(CN)_6]^{3-/4-}$ (as an electrochemical probe) in 50 mM KCl, quantified the S/N, yielding the following results: 40, 130, 170, 90, and 121 for the bare and BC, HZS_450, HZS_550, SCG_450, and SCG_550-modified electrodes, respectively. This demonstrates that biochar modification of bare electrodes significantly reduces the capacitive current (on average 3-fold decrease in comparison with bare SPE) with a consequent important improvement of the S/N ratio. Although all biochar-modified platforms exhibited enhanced performances in comparison with bare SPE, HZS_450 and HZS_550 resulted as the most promising. Afterwards, an extensive electrochemical analysis was conducted to study the electron transfer and diffusivity process occurring at the electrode of each BC-modified platform. To do this, CV and EIS were used as complementary tools for the analysis of 10 mM $[Fe(CN)_6]^{3-/4-}$.

Electroanalytical parameters, such as anodic and cathodic peak ratio (Ipa/Ipc), peak-to-peak separation (ΔE), charge transfer resistance (Rct), heterogeneous electron transfer constant (k^0) and diffusion coefficient (D_0), were evaluated and reported in Table 6.

Table 6. Comparison of the electrochemical parameters before and after biochar modification.

	Bare SPE	BC	SCG_450	SCG_550	HZS_450	HZS_550
Ipa/ Ipc	1.2±0.1	1.2±0.2	1.1±0.2	1.1±0.1	1.1±0.1	1.1±0.1
ΔE [V]	0.19±0.02	0.18±0.02	0.17±0.02	0.15±0.01	0.17±0.01	0.14±0.01
$D_0 \cdot 10^{-6}$ [cm^2/s]	1.45±0.2	2.0 ±0.2	1.9±0.1	2.4±0.2	3.5±0.1	4.2±0.2
$k^0 \cdot 10^{-3}$ [cm/s]	1.5±0.2	2.1±0.2	2.3±0.2	2.6±0.1	2.4±0.2	3.7±0.2
Ipa % Increase	/	3	30	45	60	105
Ipc % Increase	/	4	30	48	62	108

Journal Pre-proof

Rct % Decrease	/	/	10	20	40	60

From the electrochemical parameters presented in Table 6, the Ipa/Ipc ratio suggests a reversible or quasi-reversible electrochemical process (Ipa/Ipc ≈ 1). Initially, this observation might imply that the modification of SPEs with biochars (BCs) has minimal influence on the inherently sluggish surface kinetics of unmodified screen-printed electrodes. However, a more comprehensive evaluation of electrochemical parameters, such as ΔE and k^0, both of which are closely tied to electron transfer dynamics, revealed a significant enhancement associated with the drop-casting of biochar onto SPEs. Notably, all tested BCs demonstrated a decrease in ΔE and an increase in k^0 compared to the unmodified SPE (graphite-only). Among these, HZS_550 emerged as the most effective, exhibiting a twofold increase in k^0 relative to the bare electrode.

Two specific features of HZS_550 account for this: morphology and pyrolysis temperature. Regarding the first one, HZS_550 shows a more homogeneous and open structure than SCG_550, as described in section 3.2.2. This is further corroborated electrochemically through the higher diffusivity process at HZS_550-SPE (wherein the value of D_0 HZS_550 increases by a factor of two in comparison to SCG_550). In addition, D_0 calculated for HZS_550 results are comparable to the one reported in the literature by Konopka and McDuffie [77]. Thereby, a similar planar diffusion-controlled process in the oxidation/reduction reactions of the selected redox probe was found for HZS_550-modified platforms.

The second one is that the electron conductivity characteristic of biochar is strictly correlated to pyrolysis conditions. As previously reported in the literature [78] [79], the higher the pyrolysis temperature, the higher the crystallinity degree and the aromaticity rate. Indeed, at high temperatures, an improved condensation of amorphous carbon sheets can be achieved with an enhanced π-electron delocalization capacity of the material [80]. The accumulation of these conjugated π-electron systems progressively increases the conductivity of the starting material, as electrons associated with π-bonds are delocalized and become available as charge [33]. Therefore, biochar can transfer electrons directly from an electron donor to an electron acceptor without storing them. This is why the peak-to-peak separation and charge transfer resistance have decreased greatly, especially for HZS and SCG_550.

As mentioned in the pyrolysis setup section, the primary target of pyrolysis is maximizing the energy output, which leads to the choice of shorter residence time. To investigate if this choice can interfere with the

Journal Pre-proof

electrochemical behaviour of the biochar products, a subsequent thermal treatment (thermal treatment at 550°C for samples pyrolyzed originally at 550°C, residence time values of 10 and 60 min) was examined. Results show that thermal treatments on both the feedstocks did not yield satisfactory results indicating similar or even worse performances to the one already observed. **Figure 10** reports the comparison of CV obtained by comparing the performances of bare electrodes, HZS_550 and SCG_550 pre-and post-thermal treatments (TT, 60 min). CVs related to the thermal treatment of 10 minutes are not reported because the results were almost identical to HZS_550 or SCG_550. Therefore, the conductivity properties of biochar are directly linked to the initial pyrolysis conditions. It is the carbon backbone assembled during this phase which governs biochar's conductivity qualities. Post-production thermal treatment can improve the elimination of oily residues and dust, as shown in the morphological characterization section. This was confirmed by XRD analysis that was performed to investigate the structural composition of the SCG- and HZS-based biochar, before and after the post-treatment. The XRD patterns, as reported in Figure S6, are typical of carbonaceous materials such as chars and carbon blacks, with two main diffraction peaks at around 25° and 43° arising from the diffraction on the 002 and 100 crystalline planes of graphitic carbon [81]. Furthermore, diffraction peaks for the calcite ($CaCO_3$) phase are mostly evidenced in the XRD patterns of the HZS-based samples at $2\theta = 29{,}29°$ and between 39 and 49° (JCPDS: 05-0586). By comparing the 2θ positions for the 002 plane, it can be observed that the 10- and 60-min pyrolysis post-treatment led to a peak shift towards higher angles, from 23.4° to 24.9°, indicating that the interplanar distance (d_{002}) decreases according to Bragg's law. The shift is related to the formation of carbon crystalline domains [82] [83] [84]. The crystallite size along the a-axis (L_a) was estimated by deconvolution of the (100) diffraction peak, as described in the Supplementary Material (Figure S7). The highest L*a* is the greatest width of the crystallite domain. HZS_550 shows one of the highest L*a* values among the investigated samples, indicating a high crystallinity degree. On the other hand, for all samples, L*a* varies from 1.01 to 1.73 nm, indicating no significant differences in terms of crystallinity after the thermal post-treatment of HZS_550 and SCG_550.

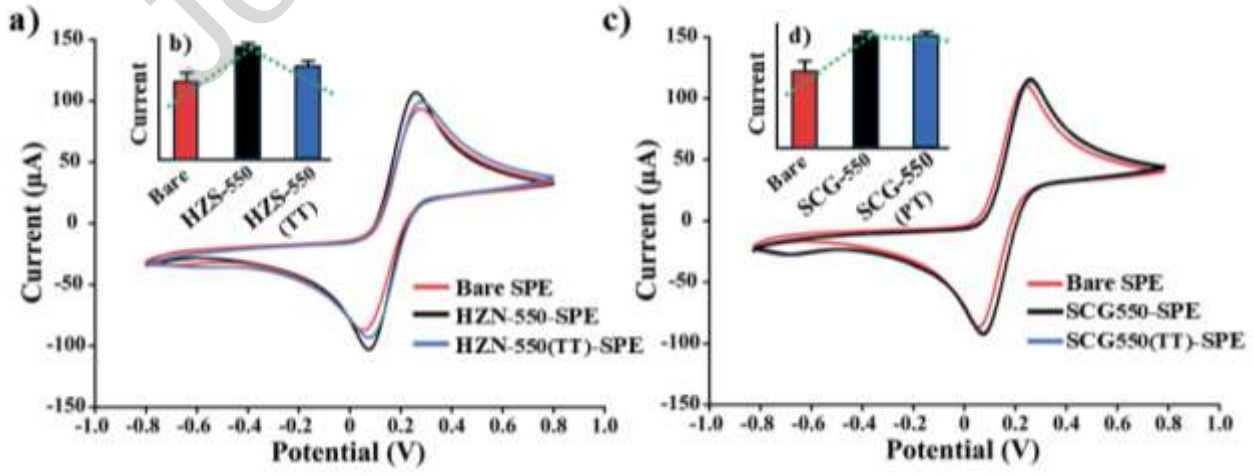

Figure 10. Electrochemical characterization of the thermal treatment effect. In a) the CVs and in b) the relative current peaks of bare, HZS_550 and HZS post-treatment-modified electrodes. In the same way, in c) and d)

the relative CVs and current peak of bare, SCG_550 and TT-SPEs were reported. An example of curves of biochar-modified-SPE fabricated sensor of at least 3 analyzed SPEs are presented (RSD%<10%).

3.4 Analytical Performances of BCs-modified SPE as sensing platforms

An electrochemical investigation was conducted on the combined conductive and adsorbent properties of HZS_550 and SCG_550 to study their sensing capabilities. Precisely, the study aims to investigate how the multilayer assembly affects the aforementioned properties, as shown in our prior research using biochar made from a different source (i.e., brewers' spent grain biochar). **Figure 11** depicts the results obtained analyzing bare SPEs, commercial biochar, SCG_550 and HZS_550-modified electrodes (with up to 4 layers - 4L) using a solution of 10 mM of $[Fe(CN)_6]^{3-/4-}$. Analyzing these platforms with a 10 mM solution of ascorbic acid yielded comparable results as a control experiment.

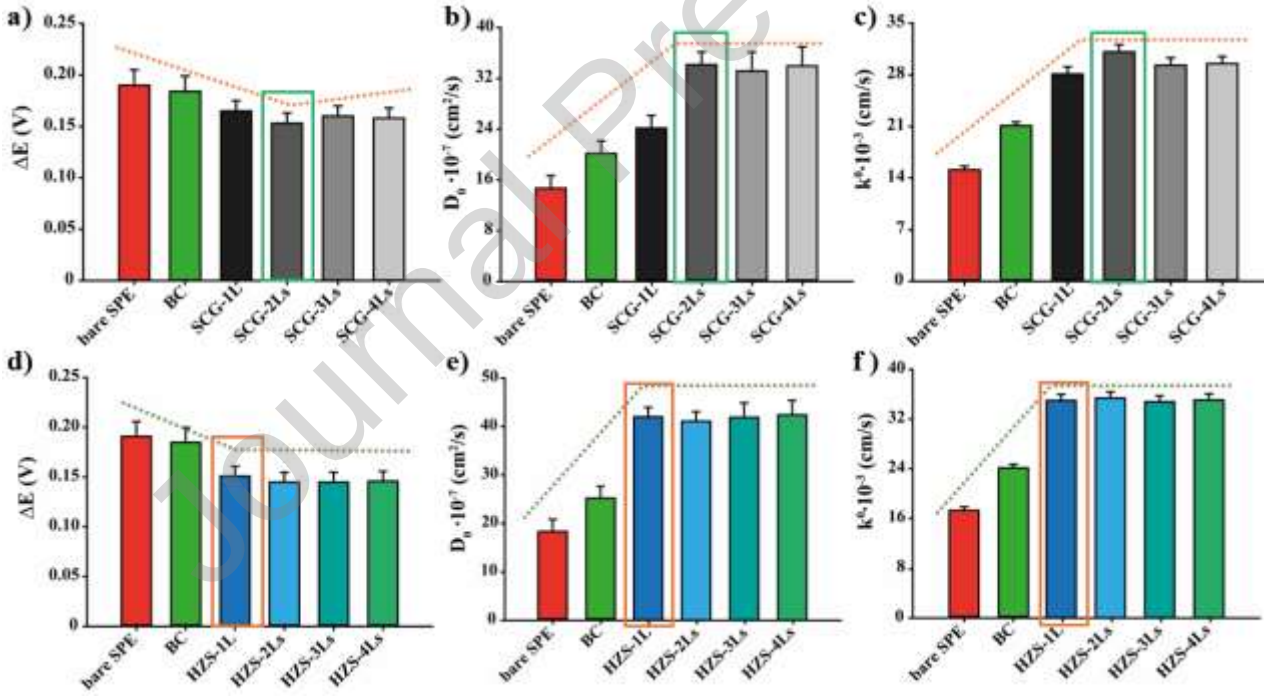

Figure 11. Electrochemical characterization of Biochar-multilayers optimization. In a), b) and c) is reported SCG_550 multilayer deposition effect on ΔE, D_0 and k^0, respectively, using $[Fe(CN)_6]^{3-/4-}$ as a reversible electroactive probe. In the same way, in d), e) and f) the outcomes relative to HZS_550 multi-layer system are reported. Each condition was studied by analyzing at least 3 SPEs with an RSD% always lower than 11%.

Journal Pre-proof

The results in **Figure 11** clearly show the distinct sensing properties of the two biochars studied. On one side, SCG_550 achieves the best sensing performances when deposited onto the working electrodes as a two-layer (SCG_550-2L) system. On the other hand, HZS_550 showed impressive performance already with just one layer (HZS_550-1L), showing relevant comparability in terms of ΔE, k^0 and D_0 between all the multilayer deposition investigated (2, 3, 4L). This is ascribable to the open texture, improved graphitization, and superior electron conductivity, as indicated by SEM and XRD analysis, testifying to HZS_550's innate applicability for sensing purposes. In light of these results, the sensing capabilities of HZS_550 and SCG_550, precisely modifying SPEs with SCG_550-2L and HZS_550-1L, have led to an evaluation of the sensing abilities using ferro-ferricyanide, ascorbic acid, nitrite, and hydroquinone as electroactive probes (concentration range 1µM to 10mM). For each analyte, the analytical performances of modified SPEs have been calculated in terms of the Limit of Detection (LOD), Limit of Quantification (LOQ), sensitivity, and repeatability. From the results reported in **Table 7**, HZS_550-1L resulted in superior sensitivity and reproducibility with all the electroactive analytes tests in water samples. Thus, demonstrating that porosity and good electron transport capability are essential qualities required for biochar to have a high sensing profile.

Table 7. Characterization of analytical performances using SWV: limit of detection (LOD), limit of quantification (LOQ), sensitivity and inter-electrode reproducibility for potassium ferricyanide, ascorbic acid, nitrite and hydroquinone for bare, SCG_550-2L and HZS_550-1L-modified SPEs.

	Bare SPE	**HZS_550-1L**	**SCG_550-2L**
$[Fe(CN)_6]^{3-/4-}$			
LOD (µM)	9.4	5.6	7.5
LOQ (µM)	31.1	18.6	24.7
Sensitivity ($\mu A/\mu M cm^2$)	40.2	29.8	36.5
Reproducibility (RSD%)	10	7	8

Ascorbic Acid			
LOD (μM)	3.4	2.6	3.2
LOQ (μM)	11.3	8.6	10.6
Sensitivity (μA/μMcm^2)	21.8	18.4	19.8
Reproducibility (RSD%)	10	8	8
NO_2^-			
LOD (μM)	20.6	7.4	15.2
LOQ (μM)	68.1	24.4	50.3
Sensitivity (μA/μMcm^2)	105.3	35.6	63.4
Reproducibility (RSD%)	11	6	9
Hydroquinone			
LOD (μM)	12.5	7.1	10.3
LOQ (μM)	41.3	21.6	32.1
Sensitivity (μA/μM cm^2)	65.4	41.3	51.7
Reproducibility (RSD%)	11	7	9

Journal Pre-proof

4. Current Challenges and Future Perspectives

Biochar-modified screen-printed sensors offer remarkable potential in analytical applications, driven by their cost-effectiveness, environmental sustainability, and exceptional electrochemical properties. These properties, however, are intrinsically linked to the structural characteristics of biochar, which are heavily influenced by preparation methods. For instance, graphitic biochar with optimized interlayer spacing is essential for sensing

and energy storage in batteries, while hierarchical porous biochar enriched with heteroatom functionalities excels in supercapacitor applications. Similarly, micropore-dominant biochar with oxygen-rich surface groups is ideal for hydrogen storage [85]. This versatility underscores biochar's near-limitless applicability. Despite their advantages, challenges persist, particularly the variability in biochar properties due to differences in feedstocks and pyrolysis conditions. This variability complicates the development of standardized preparation protocols for biochar-based (bio)sensors across diverse feedstock sources. To advance this field, future efforts should prioritize standardizing biochar production, refining functionalization techniques, and leveraging advanced nanocomposites. Scaling up these processes could unlock biochar's full potential for applications ranging from environmental monitoring to healthcare diagnostics and food safety.

5. Conclusions

Biochar application in (Bio)sensors manufacturing is currently one of the up-to-date, green, and sustainable approaches for agro-industrial waste valorization to value-added materials. This study explores the relationship between electrical conductivity, surface porosity, pyrolysis conditions, and post-production thermal treatment of biochar. With this purpose, two different feedstocks, namely HZS and SCG, were considered and investigated morphologically and electrochemically. Among all the conditions studied, HZS_550 resulted in the most effective material once deposited on the SPEs. This demonstrates that an open and well-structured texture, along with good electrical conductivity, are must-have properties for biochar to be a promising candidate for (Bio)sensing. In addition, post-production thermal treatments have no discernible influence on conductivity properties, confirming that the carbon backbone formed during the primary pyrolysis governs biochar’s electron transfer capability. Nevertheless, additional research must be undertaken to fully regulate and expand the biochar manufacturing process by its ultimate use. Consequently, this work must be regarded as a foundational building block in pursuing an advanced understanding of the biochar universe.

Acknowledgements

This was supported by “Environmental Sensing With Artificial Intelligence” project (MUR - PRIN_2022 - SENS-AI -CUP: E53D23000830006) and Grant MUR Dipartimento di Eccellenza

Journal Pre-proof

2023-27 X-CHEM project “eXpanding CHEMistry: implementing excellence in research and teaching”. This work has received funding from the European Union – Next Generation EU in response to the MUR (Ministry of University and Research) call “PRIN (Project of National Interest) 2022”: Project code: 20224WLXRK.

References

[1] A. Kumar, K. Saini, and T. Bhaskar, “Advances in design strategies for preparation of biochar based catalytic system for production of high value chemicals,” *Bioresour. Technol.*, vol. 299, no. December 2019, p. 122564, 2020, doi: 10.1016/j.biortech.2019.122564.

[2] A. A. Papa, E. Savuto, A. Di Carlo, A. Tacconi, and S. Rapagnà, “Synergic Effects of Bed Materials and Catalytic Filter Candle for the Conversion of Tar during Biomass Steam Gasification,” *Energies*, vol. 16, no. 2, pp. 1–14, 2023, doi: 10.3390/en16020595.

[3] B. Song, X. Cao, W. Gao, S. Aziz, S. Gao, C. H. Lam, and R. Lin, “Preparation of nano-biochar from conventional biorefineries for high-value applications,” *Renew. Sustain. Energy Rev.*, vol. 157, no. December 2021, p. 112057, 2022, doi: 10.1016/j.rser.2021.112057.

[4] R. H. Venderbosch and W. Prins, “Fast pyrolysis technology development,” *Biofuels, Bioprod. Biorefining*, vol. 4, no. 2, pp. 178–208, 2010, doi: 10.1002/bbb.205.

[5] L. Bartolucci, S. Cordiner, P. Mele, and V. Mulone, “Defatted spent coffee grounds fast pyrolysis polygeneration system: Lipid extraction effect on energy yield and products characteristics,” *Biomass and Bioenergy*, vol. 179, no. December 2022, p. 106974, 2023, doi: 10.1016/j.biombioe.2023.106974.

[6] E. Salehi, J. Abedi, and T. Harding, “Bio-oil from sawdust: Effect of operating parameters on the yield and quality of pyrolysis products,” *Energy and Fuels*, vol. 25, no. 9, pp. 4145–4154, 2011, doi: 10.1021/ef200688y.

[7] Z. Yi, C. Li, Q. Li, L. Zhang, S. Zhang, S. Wang, L. Qin, and X. Hu, “Influence of CO2 atmosphere on property of biochar from pyrolysis of cellulose,” *J. Environ. Chem. Eng.*, vol. 10, no. 3, p. 107339, 2022, doi: 10.1016/j.jece.2022.107339.

[8] F. Campuzano, R. C. Brown, and J. D. Martínez, “Auger reactors for pyrolysis of biomass and wastes,” *Renew. Sustain. Energy Rev.*, vol. 102, no. April 2018, pp. 372–409, 2019, doi: 10.1016/j.rser.2018.12.014.

[9] D. Chen, L. Yin, H. Wang, and P. He, “Pyrolysis technologies for municipal solid waste: A review,” *Waste Manag.*, vol. 34, no. 12, pp. 2466–2486, 2014, doi: 10.1016/j.wasman.2014.08.004.

[10] A. Di Carlo, E. Savuto, P. U. Foscolo, A. A. Papa, A. Tacconi, L. Del Zotto, B. Aydin, and E. Bocci,

Journal Pre-proof

"Preliminary Results of Biomass Gasification Obtained at Pilot Scale with an Innovative 100 kWth Dual Bubbling Fluidized Bed Gasifier," *Energies*, vol. 15, no. 12, 2022, doi: 10.3390/en15124369.

[11] R. K. Mishra and K. Mohanty, "A review of the next-generation biochar production from waste biomass for material applications," *Sci. Total Environ.*, vol. 904, no. September, p. 167171, 2023, doi: 10.1016/j.scitotenv.2023.167171.

[12] P. Premchand, D. Fino, F. Demichelis, S. Bensaid, D. Chiaramonti, G. O'Connell, J. Scott, and E. Antunes, "Synthesis of metal-free heteroatom (N, P, O, and B) doped biochar catalysts for enhanced catalytic co-pyrolysis of walnut shells and palm oil fatty acid distillate to produce high-quality bio-oil," *J. Environ. Chem. Eng.*, vol. 12, no. 5, p. 113630, 2024, doi: 10.1016/j.jece.2024.113630.

[13] L. Yan, L. Kong, Z. Qu, L. Li, and G. Shen, "Magnetic biochar decorated with ZnS nanocrytals for Pb (II) removal," *ACS Sustain. Chem. Eng.*, vol. 3, no. 1, pp. 125–132, 2015, doi: 10.1021/sc500619r.

[14] J. Fang, L. Cheng, R. Hameed, L. Jin, D. Wang, G. Owens, and D. Lin, "Release and stability of water dispersible biochar colloids in aquatic environments: Effects of pyrolysis temperature, particle size, and solution chemistry," *Environ. Pollut.*, vol. 260, p. 114037, 2020, doi: 10.1016/j.envpol.2020.114037.

[15] R. Pereira Lopes and D. Astruc, *Biochar as a support for nanocatalysts and other reagents: Recent advances and applications*, vol. 426. Elsevier B.V., 2021. doi: 10.1016/j.ccr.2020.213585.

[16] D. Yao, Q. Hu, D. Wang, H. Yang, C. Wu, X. Wang, and H. Chen, "Hydrogen production from biomass gasification using biochar as a catalyst/support," *Bioresour. Technol.*, vol. 216, pp. 159–164, 2016, doi: 10.1016/j.biortech.2016.05.011.

[17] F. Qin, C. Zhang, G. Zeng, D. Huang, X. Tan, and A. Duan, "Lignocellulosic biomass carbonization for biochar production and characterization of biochar reactivity," *Renew. Sustain. Energy Rev.*, vol. 157, no. January, p. 112056, 2022, doi: 10.1016/j.rser.2021.112056.

[18] W. J. Liu, H. Jiang, and H. Q. Yu, "Emerging applications of biochar-based materials for energy storage and conversion," *Energy Environ. Sci.*, vol. 12, no. 6, pp. 1751–1779, 2019, doi: 10.1039/c9ee00206e.

[19] S. Wang, H. Li, and M. Wu, "Advances in metal/ biochar catalysts for biomass hydro-upgrading: A review," *J. Clean. Prod.*, vol. 303, p. 126825, 2021, doi: 10.1016/j.jclepro.2021.126825.

[20] T. Pepè Sciarria, M. A. C. de Oliveira, B. Mecheri, A. D'Epifanio, J. L. Goldfarb, and F. Adani, "Metal-free activated biochar as an oxygen reduction reaction catalyst in single chamber microbial fuel cells," *J. Power Sources*, vol. 462, no. March, 2020, doi: 10.1016/j.jpowsour.2020.228183.

[21] G. Ji, Y. Xing, and T. You, "Biochar as adsorbents for environmental microplastics and nanoplastics removal," *J. Environ. Chem. Eng.*, vol. 12, no. 5, p. 113377, 2024, doi: 10.1016/j.jece.2024.113377.

[22] Z. Xiao, J. Yu, M. Feng, L. Meng, C. Yang, and W. Guo, "Three-dimensional biochar aerogel anode derived from expired yogurt for enhancing power efficiency and electron transfer at the bacteria-anode interface in microbial fuel cells," *J. Environ. Chem. Eng.*, vol. 12, no. 3, p. 113009, 2024, doi: 10.1016/j.jece.2024.113009.

Journal Pre-proof

[23] S. Anum, S. Liu, P. Zhang, A. Bostani, X. Wang, and H. Sun, “Sand-milled nanosized N-doped biochar for the efficient remediation of Pb- and Cd-contaminated soil: Preparation, performance and mechanism,” *J. Environ. Chem. Eng.*, vol. 12, no. 5, p. 114007, 2024, doi: 10.1016/j.jece.2024.114007.

[24] K. Yadav, S. Bakshi, C. Banik, D. S. Andersen, and R. C. Brown, “Assessing biochar and zeolite for enhanced agricultural sustainability of swine manure,” *J. Environ. Chem. Eng.*, vol. 12, no. 3, p. 112987, 2024, doi: 10.1016/j.jece.2024.112987.

[25] Q. U. A. Bukhari, F. Silveri, F. Della Pelle, A. Scroccarello, D. Zappi, E. Cozzoni, and D. Compagnone, “Water-Phase Exfoliated Biochar Nanofibers from Eucalyptus Scraps for Electrode Modification and Conductive Film Fabrication,” *ACS Sustain. Chem. Eng.*, vol. 9, no. 41, pp. 13988–13998, 2021, doi: 10.1021/acssuschemeng.1c05893.

[26] S. Kane, A. Storer, W. Xu, C. Ryan, and N. P. Stadie, “Biochar as a Renewable Substitute for Carbon Black in Lithium-Ion Battery Electrodes,” *ACS Sustain. Chem. Eng.*, vol. 10, no. 37, pp. 12226–12233, 2022, doi: 10.1021/acssuschemeng.2c02974.

[27] C. M. Long, M. A. Nascarella, and P. A. Valberg, “Carbon black vs. black carbon and other airborne materials containing elemental carbon: Physical and chemical distinctions,” *Environ. Pollut.*, vol. 181, pp. 271–286, 2013, doi: 10.1016/j.envpol.2013.06.009.

[28] T. Bao, Q. Wang, Y. Jiang, X. Zhao, Y. Cao, J. Cao, Q. Li, X. Ji, and W. Si, “Multicomponent nanoparticles decorating lignin-derived biochar composite for 4-nitrophenol sensing,” *J. Environ. Chem. Eng.*, vol. 12, no. 5, p. 113596, 2024, doi: 10.1016/j.jece.2024.113596.

[29] Y. Zhang, J. Zhang, K. Song, and W. Lv, “Potential of biochar derived from three biomass wastes as an electrode catalyzing oxygen reduction reaction,” *Environ. Pollut. Bioavailab.*, vol. 34, no. 1, pp. 42–50, 2022, doi: 10.1080/26395940.2021.2022538.

[30] Y. Xing, H. Zheng, C. Wang, Z. Zhang, Y. Qian, J. Qu, and X. Zhu, “Cost-efficient and ultrasensitive sensor for electrochemical detection and cytotoxicity assessment of tetracyclines,” *J. Environ. Chem. Eng.*, vol. 12, no. 5, p. 113642, 2024, doi: 10.1016/j.jece.2024.113642.

[31] R. Cancelliere, A. Di Tinno, A. M. Di Lellis, Y. Tedeschi, S. Bellucci, K. Carbone, E. Signori, G. Contini, and L. Micheli, “An inverse-designed electrochemical platform for analytical applications,” *Electrochem. commun.*, vol. 121, p. 106862, 2020, doi: 10.1016/j.elecom.2020.106862.

[32] R. Cancelliere, G. Rea, L. Severini, L. Cerri, G. Leo, E. Paialunga, P. Mantegazza, C. Mazzuca, and L. Micheli, “Expanding the circularity of plastic and biochar materials by developing alternative low environmental footprint sensors,” *Green Chem.*, vol. 25, no. 17, pp. 6774–6783, 2023, doi: 10.1039/d3gc01103h.

[33] R. Cancelliere, A. Di Tinno, A. M. Di Lellis, G. Contini, L. Micheli, and E. Signori, “Cost-effective and disposable label-free voltammetric immunosensor for sensitive detection of interleukin-6,” *Biosens. Bioelectron.*, vol. 213, no. June, p. 114467, 2022, doi: 10.1016/j.bios.2022.114467.

[34] R. Cancelliere, M. Cianciaruso, K. Carbone, and L. Micheli, “Biochar: A Sustainable Alternative in

Journal Pre-proof

the Development of Electrochemical Printed Platforms," *Chemosensors*, vol. 10, no. 8, 2022, doi: 10.3390/chemosensors10080344.

[35] N. L. Panwar and A. Pawar, "Influence of activation conditions on the physicochemical properties of activated biochar: a review," *Biomass Convers. Biorefinery*, vol. 12, no. 3, pp. 925–947, 2022, doi: 10.1007/s13399-020-00870-3.

[36] X. Xiao, B. Chen, Z. Chen, L. Zhu, and J. L. Schnoor, "Insight into Multiple and Multilevel Structures of Biochars and Their Potential Environmental Applications: A Critical Review," *Environ. Sci. Technol.*, vol. 52, no. 9, pp. 5027–5047, 2018, doi: 10.1021/acs.est.7b06487.

[37] P. Fu, W. Yi, X. Bai, Z. Li, S. Hu, and J. Xiang, "Effect of temperature on gas composition and char structural features of pyrolyzed agricultural residues," *Bioresour. Technol.*, vol. 102, no. 17, pp. 8211–8219, 2011, doi: 10.1016/j.biortech.2011.05.083.

[38] X. He, Z. Liu, W. Niu, L. Yang, T. Zhou, D. Qin, Z. Niu, and Q. Yuan, "Effects of pyrolysis temperature on the physicochemical properties of gas and biochar obtained from pyrolysis of crop residues," *Energy*, vol. 143, pp. 746–756, 2018, doi: 10.1016/j.energy.2017.11.062.

[39] W. J. Liu, H. Jiang, and H. Q. Yu, "Development of Biochar-Based Functional Materials: Toward a Sustainable Platform Carbon Material," *Chem. Rev.*, vol. 115, no. 22, pp. 12251–12285, 2015, doi: 10.1021/acs.chemrev.5b00195.

[40] F. G. de Mendonça, I. T. da Cunha, R. R. Soares, J. C. Tristão, and R. M. Lago, "Tuning the surface properties of biochar by thermal treatment," *Bioresour. Technol.*, vol. 246, no. July, pp. 28–33, 2017, doi: 10.1016/j.biortech.2017.07.099.

[41] S. Fiori, F. Della Pelle, F. Silveri, A. Scroccarello, E. Cozzoni, M. Del Carlo, and D. Compagnone, "Nanofibrillar biochar from industrial waste as hosting network for transition metal dichalcogenides. Novel sustainable 1D/2D nanocomposites for electrochemical sensing," *Chemosphere*, vol. 317, no. December 2022, p. 137884, 2023, doi: 10.1016/j.chemosphere.2023.137884.

[42] W. S. Devi, R. Kaur, A. Sharma, S. Thakur, S. K. Mehta, V. Raja, and F. S. Ataya, "Non-enzymatic g-C3N4 supported CuO derived-biochar based electrochemical sensors for trace level detection of malathion," *Biosens. Bioelectron.*, vol. 267, no. June 2024, p. 116808, 2025, doi: 10.1016/j.bios.2024.116808.

[43] M. G. P. Valenga, A. Gevaerd, L. H. Marcolino-Junior, and M. F. Bergamini, "Biochar from sugarcane bagasse: Synthesis, characterization, and application in an electrochemical sensor for copper (II) determination," *Biomass and Bioenergy*, vol. 184, no. September 2023, 2024, doi: 10.1016/j.biombioe.2024.107206.

[44] S. Allende, Y. Liu, and M. V. Jacob, "Electrochemical sensing of paracetamol based on sugarcane bagasse-activated biochar," *Ind. Crops Prod.*, vol. 211, no. February, p. 118241, 2024, doi: 10.1016/j.indcrop.2024.118241.

[45] R. Wang, X. Lan, T. Zhou, X. Qian, B. Qu, P. Lv, and Y. Wang, "Detection of chloramphenicol in dairy products based on biogas residue biochar based electrochemical sensor," *J. Food Compos.*

Journal Pre-proof

Anal., vol. 125, no. August 2023, p. 105824, 2024, doi: 10.1016/j.jfca.2023.105824.

[46] M. Zhang, Y. Wang, B. You, Z. Qi, Y. Wang, and Z. Zhang, "Nickel oxide decorated popcorn derived biochar as a non-invasive electrochemical sensor for sensitive detection of glucose in saliva," *J. Alloys Compd.*, vol. 1010, no. August 2024, p. 177427, 2025, doi: 10.1016/j.jallcom.2024.177427.

[47] S. A. Kim, E. B. Kim, M. Imran, K. Shahzad, D. H. Moon, M. S. Akhtar, S. Ameen, and S. H. Park, "Naturally manufactured biochar materials based sensor electrode for the electrochemical detection of polystyrene microplastics," *Chemosphere*, vol. 351, no. August 2023, p. 141151, 2024, doi: 10.1016/j.chemosphere.2024.141151.

[48] J. de O. S. Silva, J. F. dos Santos, H. S. Granja, W. S. Almeida, T. F. L. Loeser, L. S. Freitas, M. F. Bergamini, L. H. Marcolino-Junior, and E. M. Sussuchi, "Simultaneous determination of carbendazim and carbaryl pesticides in water bodies samples using a new voltammetric sensor based on Moringa oleifera biochar," *Chemosphere*, vol. 347, no. July 2023, 2024, doi: 10.1016/j.chemosphere.2023.140707.

[49] Z. Su, J. Wang, S. Hu, Y. Cheng, Y. Yang, S. Zhou, M. Chen, Q. Cao, S. Zhang, L. Yang, Z. Liu, and X. Tu, "In-situ reshaping nano-biochar on electrode surface for machine learning assisted selective sensing of Pb2+ in real water samples," *Appl. Surf. Sci.*, vol. 665, no. April, p. 160294, 2024, doi: 10.1016/j.apsusc.2024.160294.

[50] C. Kalinke, P. R. de Oliveira, L. H. Marcolino-Júnior, and M. F. Bergamini, "Nanostructures of Prussian blue supported on activated biochar for the development of a glucose biosensor," *Talanta*, vol. 274, no. April, 2024, doi: 10.1016/j.talanta.2024.126042.

[51] S. Di Fraia, S. Fabozzi, A. Macaluso, and L. Vanoli, "Energy potential of residual biomass from agro-industry in a Mediterranean region of southern Italy (Campania)," *J. Clean. Prod.*, vol. 277, p. 124085, 2020, doi: 10.1016/j.jclepro.2020.124085.

[52] J. R. Banu, S. Kavitha, R. Y. Kannah, M. D. Kumar, and A. E. Atabani, "Bioresource Technology Biore fi nery of spent co ff ee grounds waste : Viable pathway towards circular bioeconomy," vol. 302, no. January, 2020, doi: 10.1016/j.biortech.2020.122821.

[53] L. Bartolucci, S. Cordiner, A. Di Carlo, A. Gallifuoco, P. Mele, and V. Mulone, "Platform chemicals recovery from spent coffee grounds aqueous-phase pyrolysis oil," *Renew. Energy*, vol. 220, no. February 2023, p. 119630, 2024, doi: 10.1016/j.renene.2023.119630.

[54] S. Kelkar, C. M. Saffron, L. Chai, J. Bovee, T. R. Stuecken, M. Garedew, Z. Li, and R. M. Kriegel, "Pyrolysis of spent coffee grounds using a screw-conveyor reactor," *Fuel Process. Technol.*, vol. 137, pp. 170–178, 2015, doi: 10.1016/j.fuproc.2015.04.006.

[55] E. P. Putun, A.E, A. Ozcan, "Pyrolysis of hazelnut shells in a fixed-bed tubular reactor: yields and structural analysis of bio-oil," *J. Anal. Appl. Pyrolysis*, vol. 52, pp. 33–49, 1999, [Online]. Available: www.elsevier.com/locate/jaap

[56] P. M. and V. Lorenzo Bartolucci, Stefano Cordiner, Gopalakrishnan Kumar and Mulone, "Intermediate pyrolysis of hazelnut shell: temperature effect on energy conversion and products

Journal Pre-proof

characteristics," pp. 1–22, 2024, [Online]. Available: https://www.researchsquare.com/article/rs-4292816/latest

[57] A. M. Parvez, M. T. Afzal, P. Jiang, and T. Wu, "Microwave-assisted biomass pyrolysis polygeneration process using a scaled-up reactor: Product characterization, thermodynamic assessment and bio-hydrogen production," *Biomass and Bioenergy*, vol. 139, no. June 2019, p. 105651, 2020, doi: 10.1016/j.biombioe.2020.105651.

[58] C. T. Primaz, T. Schena, E. Lazzari, E. B. Caramão, and R. A. Jacques, "Influence of the temperature in the yield and composition of the bio-oil from the pyrolysis of spent coffee grounds: Characterization by comprehensive two dimensional gas chromatography," *Fuel*, vol. 232, no. June, pp. 572–580, 2018, doi: 10.1016/j.fuel.2018.05.097.

[59] Z. Gökdai, A. Sinağ, and T. Yumak, "Comparison of the catalytic efficiency of synthesized nano tin oxide particles and various catalysts for the pyrolysis of hazelnut shell," *Biomass and Bioenergy*, vol. 34, no. 3, pp. 402–410, 2010, doi: 10.1016/j.biombioe.2009.12.003.

[60] F. Ronsse, S. van Hecke, D. Dickinson, and W. Prins, "Production and characterization of slow pyrolysis biochar: Influence of feedstock type and pyrolysis conditions," *GCB Bioenergy*, vol. 5, no. 2, pp. 104–115, 2013, doi: 10.1111/gcbb.12018.

[61] C. Di Blasi, A. Galgano, and C. Branca, "Exothermic Events of Nut Shell and Fruit Stone Pyrolysis," *ACS Sustain. Chem. Eng.*, vol. 7, no. 9, pp. 9035–9049, 2019, doi: 10.1021/acssuschemeng.9b01474.

[62] M. Aysla Costa De Oliveira, A. D'Epifanio, H. Ohnuki, and B. Mecheri, "Platinum group metal-free catalysts for oxygen reduction reaction: Applications in microbial fuel cells," *Catalysts*, vol. 10, no. 5, pp. 1–22, 2020, doi: 10.3390/catal10050475.

[63] X. Zhu, C. Li, J. Li, B. Xie, J. Lü, and Y. Li, "Thermal treatment of biochar in the air/nitrogen atmosphere for developed mesoporosity and enhanced adsorption to tetracycline," *Bioresour. Technol.*, vol. 263, no. May, pp. 475–482, 2018, doi: 10.1016/j.biortech.2018.05.041.

[64] H. Haykiri-Acma, A. Baykan, S. Yaman, and S. Kucukbayrak, "Effects of fragmentation and particle size on the fuel properties of hazelnut shells," *Fuel*, vol. 112, pp. 326–330, 2013, doi: 10.1016/j.fuel.2013.05.051.

[65] R. Changotra, H. Rajput, J. Yang, M. Dasog, and Q. (Sophia) He, "Spent-coffee grounds-derived biochar-supported heterogeneous photocatalyst: a performance evaluation and mechanistic approach for the degradation of pentachlorophenol," *RSC Sustain.*, vol. 1, no. 6, pp. 1484–1496, 2023, doi: 10.1039/d3su00153a.

[66] T. S. Andrade, J. Vakros, D. Mantzavinos, and P. Lianos, "Biochar obtained by carbonization of spent coffee grounds and its application in the construction of an energy storage device," *Chem. Eng. J. Adv.*, vol. 4, no. November, p. 100061, 2020, doi: 10.1016/j.ceja.2020.100061.

[67] A. Panahi, N. Vorobiev, M. Schiemann, M. Tarakcioglu, M. Delichatsios, and Y. A. Levendis, "Combustion details of raw and torrefied biomass fuel particles with individually-observed size, shape and mass," *Combust. Flame*, vol. 207, pp. 327–341, 2019, doi:

Journal Pre-proof

10.1016/j.combustflame.2019.06.009.

[68] D. Chen, X. Zhuang, Z. Gan, K. Cen, Y. Ba, and D. Jia, "Co-pyrolysis of light bio-oil leached bamboo and heavy bio-oil: Effects of mass ratio, pyrolysis temperature, and residence time on the biochar," *Chem. Eng. J.*, vol. 437, no. P1, p. 135253, 2022, doi: 10.1016/j.cej.2022.135253.

[69] V. N. Nguyen, P. Sharma, L. Rowinski, H. C. Le, D. T. N. Le, S. M. Osman, H. S. Le, T. H. Truong, P. Q. P. Nguyen, and D. N. Cao, "Biochar-based catalysts derived from biomass waste: production, characterization, and application for liquid biofuel synthesis," *Biofuels, Bioprod. Biorefining*, vol. 18, no. 2, pp. 594–616, 2024, doi: 10.1002/bbb.2593.

[70] E. W. Bruun, H. Hauggaard-Nielsen, N. Ibrahim, H. Egsgaard, P. Ambus, P. A. Jensen, and K. Dam-Johansen, "Influence of fast pyrolysis temperature on biochar labile fraction and short-term carbon loss in a loamy soil," *Biomass and Bioenergy*, vol. 35, no. 3, pp. 1182–1189, 2011, doi: 10.1016/j.biombioe.2010.12.008.

[71] T. Ohra-aho, C. Lindfors, J. Lehtonen, T. Tamminen, and V. Siipola, "Activated Carbons from Fast Pyrolysis Biochar as Novel Catalysts for the Post-Treatment of Pyrolysis Vapors, Studied by Analytical Pyrolysis," *C*, vol. 6, no. 4, p. 65, 2020, doi: 10.3390/c6040065.

[72] R. Janu, V. Mrlik, D. Ribitsch, J. Hofman, P. Sedláček, L. Bielská, and G. Soja, "Biochar surface functional groups as affected by biomass feedstock, biochar composition and pyrolysis temperature," *Carbon Resour. Convers.*, vol. 4, no. November 2020, pp. 36–46, 2021, doi: 10.1016/j.crcon.2021.01.003.

[73] M. Keiluweit, P. S. Nico, M. Johnson, and M. Kleber, "Dynamic molecular structure of plant biomass-derived black carbon (biochar)," *Environ. Sci. Technol.*, vol. 44, no. 4, pp. 1247–1253, 2010, doi: 10.1021/es9031419.

[74] F. J. Calderón, G. W. McCarty, and J. B. Reeves, "Pyrolisis-MS and FT-IR analysis of fresh and decomposed dairy manure," *J. Anal. Appl. Pyrolysis*, vol. 76, no. 1–2, pp. 14–23, 2006, doi: 10.1016/j.jaap.2005.06.009.

[75] X. Cao and W. Harris, "Properties of dairy-manure-derived biochar pertinent to its potential use in remediation," *Bioresour. Technol.*, vol. 101, no. 14, pp. 5222–5228, 2010, doi: 10.1016/j.biortech.2010.02.052.

[76] V. Bejenari, A. Marcu, A. M. Ipate, D. Rusu, N. Tudorachi, I. Anghel, I. E. Şofran, and G. Lisa, "Physicochemical characterization and energy recovery of spent coffee grounds," *J. Mater. Res. Technol.*, vol. 15, pp. 4437–4451, 2021, doi: 10.1016/j.jmrt.2021.10.064.

[77] S. J. Konopka and B. McDuffie, "Diffusion Coefficients of Ferri- and Ferrocyanide Ions in Aqueous Media, Using Twin-Electrode Thin-Layer Electrochemistry," *Anal. Chem.*, vol. 42, no. 14, pp. 1741–1746, 1970, doi: 10.1021/ac50160a042.

[78] P. Kim, A. Johnson, C. W. Edmunds, M. Radosevich, F. Vogt, T. G. Rials, and N. Labbé, "Surface functionality and carbon structures in lignocellulosic-derived biochars produced by fast pyrolysis," *Energy and Fuels*, vol. 25, no. 10, pp. 4693–4703, 2011, doi: 10.1021/ef200915s.

Journal Pre-proof

[79] A. M. Dehkhoda, N. Ellis, and E. Gyenge, "Electrosorption on activated biochar: Effect of thermo-chemical activation treatment on the electric double layer capacitance," *J. Appl. Electrochem.*, vol. 44, no. 1, pp. 141–157, 2014, doi: 10.1007/s10800-013-0616-4.

[80] M. Bartoli, M. Troiano, P. Giudicianni, D. Amato, M. Giorcelli, R. Solimene, and A. Tagliaferro, "Effect of heating rate and feedstock nature on electrical conductivity of biochar and biochar-based composites," *Appl. Energy Combust. Sci.*, vol. 12, no. May, p. 100089, 2022, doi: 10.1016/j.jaecs.2022.100089.

[81] N. M. Keppetipola, M. Dissanayake, P. Dissanayake, B. Karunarathne, M. A. Dourges, D. Talaga, L. Servant, C. Olivier, T. Toupance, S. Uchida, K. Tennakone, G. R. A. Kumara, and L. Cojocaru, "Graphite-type activated carbon from coconut shell: a natural source for eco-friendly non-volatile storage devices," *RSC Adv.*, vol. 11, no. 5, pp. 2854–2865, 2021, doi: 10.1039/d0ra09182k.

[82] C. V. C. Sreeprasanth Pulinthanathu Sree, A. a Wauter Wangermez, b M. B. J. R. Gina Vanbutsele, a Jin Won Seo, a E. Breynaert, A, and and J. A. Martens, "Low-temperature activation of carbon black by selective photocatalytic oxidation," *Nanoscale Adv.*, vol. 1, no. 8, pp. 2873–2880, 2019, doi: 10.1039/c9na00188c.

[83] E. Pusceddu, S. F. Santilli, G. Fioravanti, A. Montanaro, F. Miglietta, and P. U. Foscolo, "Chemical-physical analysis and exfoliation of biochar-carbon matter: From agriculture soil improver to starting material for advanced nanotechnologies," *Mater. Res. Express*, vol. 6, no. 11, 2019, doi: 10.1088/2053-1591/ab4ba8.

[84] V. Asokan, V. Venkatachalapathy, K. Rajavel, and D. N. Madsen, "Microwave irradiation on carbon black: Studies on the transformation of particles into nano-balls, nano-sticks and nano-onion like structures," *J. Phys. Chem. Solids*, vol. 99, pp. 173–181, 2016, doi: 10.1016/j.jpcs.2016.09.002.

[85] T. B. Shivam Rawat, Chin-Tsan Wang, Chyi-How Lay, Srinivas Hotha, "Sustainable biochar for advanced electrochemical/energy storage applications," *J. Energy Storage*, vol. 63, no. January, p. 107115, 2023, doi: 10.1016/j.est.2023.107115.

Journal Pre-proof

Journal Pre-proof

Declaration of interests

☐ The authors declare that they have no known competing financial interests or personal relationships that could have appeared to influence the work reported in this paper.

☒ The authors declare the following financial interests/personal relationships which may be considered as potential competing interests:

Laura Micheli reports financial support was provided by MUR. If there are other authors, they declare that they have no known competing financial interests or personal relationships that could have appeared to influence the work reported in this paper.

Journal Pre-proof